Applied Catalysis B: Environmental 327 (2023) 122455

Contents lists available at ScienceDirect

Applied Catalysis B: Environmental

journal homepage: www.elsevier.com/locate/apcatb

NO_x storage and reduction by H_2 over highly dispersed Pt on $Co_1Mg_2Al_1O_x$-LDO for stationary applications: A transient kinetic study

Cheng Zhang [a,b], Constantinos M. Damaskinos [c], Michalis A. Vasiliades [c], Yuefeng Liu [d], Qian Jiang [d], Qiang Wang [a,b,*], Angelos M. Efstathiou [c,**]

[a] Beijing Key Lab for Source Control Technology of Water Pollution, College of Environmental Science and Engineering, Beijing Forestry University, Beijing 100083, PR China

[b] Engineering Research Center for Water Pollution Source Control & Eco-remediation, College of Environmental Science and Engineering, Beijing Forestry University, Beijing 100083, PR China

[c] Chemistry Department, Heterogeneous Catalysis Laboratory, University of Cyprus, 1 University Ave., University Campus, 2109 Nicosia, Cyprus

[d] Dalian National Laboratory for Clean Energy, Dalian Institute of Chemical Physics, Chinese Academy of Sciences, Dalian 116023, PR China

ARTICLE INFO

Keywords:
Layered double hydroxides (LDHs)
NO_x storage
Supported Pt catalyst
Transient kinetics
NO_x reduction by H_2

ABSTRACT

The performance of a highly dispersed Pt/$Co_1Mg_2Al_1O_x$-LDO catalyst towards NO_x-storage and reduction by H_2 for NO_x control in stationary applications was investigated under forced feed composition cycling ("swing-reactor" system). The influence of 7 vol% CO_2 and 5 vol% H_2O in the NO-containing and H_2-containing feeds on the dynamic evolution of adsorbed NO_x-s and their reduction performance (conversion and N_2-selectvity) were determined in the 200–400 °C range. The effects of catalyst pretreatment with 20 or 50 ppm SO_2/He gas mixture on its NO_x-s storage and reduction by hydrogen dynamics were also investigated. Reduction of NO_x-s formed on the support involves a hydrogen spillover effect from Pt to the metal-support interface and support NO_x-s sites. A very stable NSR performance was obtained at 350 °C for 2 h of successive NO_x-adsorption (3 min)/reduction by H_2 (1 min) steps. The nature of active and inactive NO_x-s in H_2 was probed by in-situ DRIFTS.

1. Introduction

NO_x storage and reduction (NSR) has been initially considered as an efficient and promising approach for removing NO_x from lean-burn engines (mobile applications, lean NO_x trap, LNT) [1–5]. NSR has also been proposed lately as a promising de-NO_x technology for removing NO_x from industrial flue gas streams (stationary applications), considering the low NO_x concentrations (50–100 ppm) and the on-site availability of H_2 (e.g., naphtha cracker units) [5,6]. In this proposed NSR-stationary NO_x control technology, periodic injections of a low-concentration H_2 gas stream over a bifunctional NO_x-storage and H_2-SCR material might turn out to be an alternative approach with lower cost compared to the current NH_3-SCR (stationary sources; T = 300–350 °C) [7,8]. Scheme 1**a** suggests a potential flowsheet of the proposed deNO_x process (stationary applications) operated under forced feed composition cycling with a "swing-reactor" system consisting of two catalytic reactors [9,10]. For this, the NO_x-containing flue gas stream passes first through Reactor R1 containing an efficient catalyst for NO_x adsorption as depicted in Scheme 1**b**. After the effluent gas stream reaches a predetermined and allowable NO_x concentration according to the breakthrough curve, the effluent gas stream is directed to reactor R2, while at the same time reactor R1 is switched (use of SV1, 3-way valve) to a hydrogen gas stream of low-concentration for the selective reduction of pre-adsorbed NO_x to N_2 and H_2O as depicted in Scheme 1**c**. For lowering the cost of hydrogen usage for practical applications, this could be envisioned by keeping the reactor in air and not in hydrogen gas stream after the NO_x reduction step (Scheme 1c). Therefore, appropriate catalyst compostion is required to perform NO_x adsorption over a partially/fully oxidized and not fully reduced (use of H_2) state of it. In the present work, this important issue was realized successfully on a 0.59 wt % Pt/$Co_1Mg_2Al_1O_x$-LDO catalyst along with the other NSR process steps.

The NSR catalytic systems installed in lean-burn internal combustion engines consist of precious metal (Pt) for effective NO oxidation and reduction of the NO_x-s species, and of NO_x storage components [2–4,

* Corresponding author at: Beijing Key Lab for Source Control Technology of Water Pollution, College of Environmental Science and Engineering, Beijing Forestry University, Beijing 100083, PR China.

** Corresponding author.

E-mail addresses: qiangwang@bjfu.edu.cn (Q. Wang), efstath@ucy.ac.cy (A.M. Efstathiou).

https://doi.org/10.1016/j.apcatb.2023.122455
Received 17 July 2022; Received in revised form 16 January 2023; Accepted 8 February 2023
Available online 10 February 2023

11–13]. Considering the high price of Pt, transition metal oxides with strong oxidative properties might be considered as very good potential substitutes. Among them, cobalt oxide has been extensively investigated [5,14,15]. Wang et al. [14] investigated the effect of Co addition in a commercial Pt/BaO-Al_2O_3 catalytic system on its LNT performance. An improved NO oxidation efficiency and an increased NO_x storage capacity was reported, leading to higher N_2-selectvity values compared to the unpromoted catalyst. Co-containing perovskites also exhibited comparable performance with Pt-based catalysts due to their high NO oxidation activity [16].

High metal (Pt, Ir) dispersion was reported [17,18] to effectively promote the selective reduction of NO_x-s to N_2(g) by CO or H_2. The development of highly dispersed, including single-atom metal catalysts, might therefore be a promising strategy for NSR when combined with H_2 reducing agent. Lin et al. [19] developed a Pt_1 (single atom)/FeO_x catalyst for NO reduction by H_2 which exhibited significantly higher NO conversion and N_2 selectivity than other supported Pt nanocatalysts. The improved de-NO_x performance was attributed not only to the stronger NO adsorption and easier dissociation of the N-O bond but also to the presence of an increased concentration of oxygen vacancies in the FeO_x support. There are no reports on highly dispersed Pt-based NSR (use of H_2) catalytic systems to the best of our knowledge.

The transient response method has long been appreciated and acknowledged as a very powerful technique for gaining deeper insight into kinetic and mechanistic aspects of heterogeneous catalytic reactions [20,21]. Efstathiou and his group [7,17,22–24] conducted several studies on lean de-NO_x reactions using hydrogen as reducing agent, where Steady State Isotopic Transient Kinetic Analysis (SSITKA) coupled with DRIFTS was applied to identify the chemical structure of active and inactive (spectator) NO_x adsorbed species, and estimate the surface coverage (θ) of *active* NO_x-s. Based on the magnitude of θ, it was possible to prove the bifunctional character of the catalyst for NO_x reduction by hydrogen (site location of active NO_x-s). Tronconi and his group [1, 25–27] also conducted several studies on NO_x control, including Lean NO_x Trap, NH_3-SCR, and NO oxidation using the transient response method. For example, the step-gas concentration switch $NO/O_2 \rightarrow He$ (t) or H_2 (t) proved that nitrates stored on Pt/Ba/Al_2O_3 (NSR catalyst) were reduced without involving thermal decomposition of adsorbed NO_x as a preliminary step [27]. Several other groups [28–31] have also applied the transient response method coupled with microkinetic modeling and IR spectroscopy to better understand the LNT performance with H_2 as reducing agent.

Layered double hydroxides (LDHs) is a class of layered structure solids that have been studied in the deNO_x field [5,6,32]. After thermal treatment, the obtained layered double oxides (LDOs) are generally of high basicity and specific surface area, which potentially become ideal supports of the active catalytic phase for NSR.

In the present work, highly dispersed Pt (large part of deposited Pt exists as single atoms and/or very small clusters of few atoms) on $Co_1Mg_2Al_1O_x$-LDO was prepared and tested as a potential NSR catalyst for NO_x control using hydrogen as reducing agent for stationary applications, according to the design concepts presented in Scheme 1. A series of transient kinetic experiments were conducted and analyzed to gather fundamental information related to the transient NO adsorption behavior (*NO_x storage* process step) and the transient evolution of N-containing species during the *NO_x reduction by H_2* process step. The influence of H_2 concentration and the presence of 5% H_2O/7% CO_2 in the H_2-containing feed gas stream on the NO_x reduction by H_2 kinetics, and

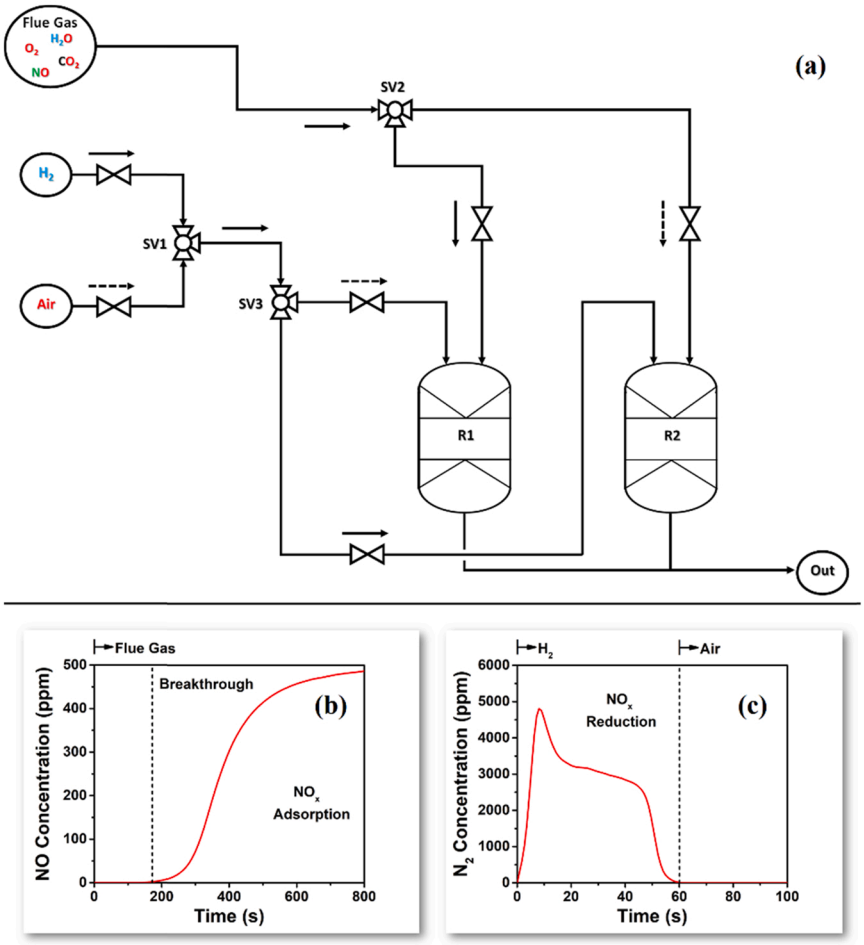

Scheme 1. (a) Flowsheet of a two parallel flow catalytic bed reactor systems, where NO_x adsorption (e.g., R1 running flue gas) and NO_x reduction (R2, running H_2 gas stream) can be applied at the same time (use of SV1-SV3 three-way valves). Transient concentration response curves of NO reactant (b), and N_2 gas product (c) obtained at 300 °C during the step-gas switch He → 0.1% NO/10% O_2/1% Kr/He (20 min) (NO_x adsorption step, Scheme 1b), followed by the step-gas switch He → 5% H_2/He (T, t) (NO_x reduction step, Scheme 1c) over the Pt/$Co_1Mg_2Al_1O_x$-LDO catalyst.

that of 5% H_2O/7% CO_2 and 20 or 50 ppm SO_2 on the NO_x storage performance were systematically investigated. The present work provided very insightful information about the NSR performance and its associated transient kinetics on a potential $Co_1Mg_2Al_1O_x$-LDO supported Pt nanocatalyst for NO_x control used in stationary source applications with *hydrogen* as reducing agent, for the first time to the best of our knowledge. This work paves the way for future development of efficient LDO-based materials for industrial NO_x control with on-site H_2 availability.

2. Experimental

2.1. Synthesis of supported Pt catalyst

The $Co_1Mg_2Al_1$-CO_3 LDH (Co: Mg:Al = 1: 2: 1) support with Pt deposited on it was synthesized by the co-precipitation method [6]. Metal precursor solutions of $Co(NO_3)_2{\cdot}6\,H_2O$ (0.025 M), $Mg(NO_3)_2{\cdot}6\,H_2O$ (0.05 M), $Al(NO_3)_3{\cdot}9\,H_2O$ (0.025 M) and a given amount of $H_2PtCl_6{\cdot}6\,H_2O$ (Pt/$Co_1Mg_2Al_1$-CO_3 LDH synthesis) were dissolved in deionized water (100 mL) at 27 °C and stirred for 10 min. The resulting homogeneous aqueous solution was then added dropwise to a continuously stirred basic solution (100 mL) containing 0.05 M Na_2CO_3. The pH value of the resulting liquid mixture was maintained at ~ 10 by adding dropwise NaOH solution (4 M). After aging at room temperature for 12 h, the obtained slurry was filtered and washed with deionized water until pH = 7. The obtained samples in powder form (filter cake) were then dispersed in ethanol under stirring for 2 h and then washed with ethanol thoroughly. The samples were subsequently dried at 60 °C overnight to obtain $Co_1Mg_2Al_1$-CO_3 LDH (without the addition of $H_2PtCl_6{\cdot}6\,H_2O$) and Pt/$Co_1Mg_2Al_1$-CO_3 LDH solid products. After calcination at 500 °C/5 h in static air (furnace), $Co_1Mg_2Al_1O_x$-LDO and Pt/$Co_1Mg_2Al_1O_x$-LDO solids were obtained and stored for further use.

2.2. Characterization of supported Pt catalyst

2.2.1. Pt metal loading and dispersion

The Pt metal loading of Pt/$Co_1Mg_2Al_1O_x$-LDO catalyst was measured by inductively coupled plasma-mass spectrometry (7900 ICP-MS, Agilent), while the mean Pt particle size (d_{Pt}, nm) by H_2 chemisorption followed by TPD, and also by STEM imaging (Section 2.2.2). For hydrogen chemisorption/TPD, the Pt/$Co_1Mg_2Al_1O_x$-CO_3 LDO (0.3 g) was first pretreated in situ with 20 vol% O_2/He (50 NmL min^{-1}) at 500 °C/2 h, followed by He purge until the O_2 MS-signal reached its background value. The catalyst was then cooled in He gas flow to 400 °C and reduced in 5 vol% H_2/He for 2 h followed by He purge. The reactor was then cooled quickly in He gas flow to 30 °C followed by 30-min exposure to a 0.5 vol% H_2/He adsorption gas. The sample was then purged in He flow (50 NmL min^{-1}) for 10 min and the temperature of the solid was increased to 500 °C (β = 30 °C min^{-1}). During TPD, the H_2 signal (m/z = 2) was continuously monitored with *on-line* mass spectrometer (MS, Balzers, Omnistar 1–200 amu) and converted into concentration (ppm) after using a certified gas mixture (0.95 vol% H_2/He). Metal dispersion (D_{Pt}, %) was estimated after considering an H_2 chemisorption stoichiometry of H/Pt_s = 1. A Pt mean particle size, d_{Pt} (nm) was estimated assuming hemispherical particles and using the following relationship [33]:

$$d_{Pt}(nm) = \frac{1.1}{D_{Pt}} \quad (1)$$

A hydrogen spillover effect was checked by increasing the concentration of H_2 in the adsorption gas mixture to 1 vol% and the time of adsorption to 1 h. No additional chemisorption was found within experimental error based on the H_2-TPD trace recorded.

2.2.2. Structure and texture analysis

Powder X-ray diffraction patterns of the support alone (LDH or LDO) and of the corresponding calcined supported Pt catalyst were recorded on the XRD-7000 diffractometer (Shimadzu, Cu Kα radiation). The specific surface area (SSA, $m^2\,g^{-1}$), pore volume (V_p, $cm^3\,g^{-1}$) and mean pore diameter (d_p, nm) of the solids were measured based on the N_2 adsorption/desorption isotherms at 77 K (SSA-7000, Builder). Scanning transmission electron microscopy (STEM) imaging and energy dispersive X-ray (EDX) analysis were performed on a Hitachi HF 5000 microscope with a 200 kV cold-field emission gun and Cs corrector for the electron probe.

2.2.3. In situ DRIFTS - NO_x adsorption and transient H_2 reduction studies

In situ DRIFTS-NO adsorption followed by transient H_2 reduction studies were conducted on a Perkin-Elmer Frontier FT-IR spectrometer (averaged spectrum of 256 scans, resolution of 4 cm^{-1}, scanning speed rate of 2 cm s^{-1}, MCT detector) coupled with a temperature controllable DRIFTS reactor cell (Harrick Scientific, Praying Mantis) equipped with CaF_2 windows. The sample after grinding and sieving (< 106 μm in size; fine powder form) was placed in the DRIFTS cell. The temperature of the sample was then increased in 5% H_2/He gas flow to 400 °C and kept at 400 °C/1 h, then the sample was purged in Ar while its temperature was decreased gradually from 400 to 200 °C to record background spectra in Ar and 5% H_2/He gas flow at 400, 300 and 200 °C. The feed gas was subsequently switched to 0.1% NO/10% O_2/He (50 NmL min^{-1}) at the desired T, and DRIFTS spectra were recorded every 15 s. The transient isothermal reduction of adsorbed NO_x-s by H_2 at a given temperature was conducted by performing the step-gas switch He → 5 vol% H_2/He (T, t), following NO/O_2/He gas treatment of the solid and a 3-min He purge. DRIFTS spectra were recorded under H_2/He gas treatment.

2.3. Transient NO_x storage and reduction - Mass spectrometry

Transient kinetic experiments for studying the dynamics of adsorption and reduction of NO_x-s by H_2 over the Pt/$Co_1Mg_2Al_1O_x$-LDO catalyst were performed in a home-made transient gas-flow system equipped with a CSTR micro-reactor previously described [34]. The transient adsorption kinetic behavior of NO was investigated in the 200–400 °C range according to the following step-gas concentration switches:

(i) He → 0.1 vol% NO/1 vol% Kr/He (T, t)
(ii) He → 0.1 vol% NO/10 vol% O_2/x vol% H_2O and/or 7 vol% CO_2/1 vol% Kr/He (T, t); x = 0 or 5.

The transient isothermal hydrogenation (TIH) of NO_x-s (NO_x reduction) was studied following step (ii), according to the following sequence of step-gas switches:

(iii) 0.1 vol% NO/10 vol% O_2/x vol% H_2O/1 vol% Kr/He (T, 20 min) → He (3 min) → 5 vol% H_2/x vol% H_2O and/or 7 vol% CO_2/He (t); x = 0 or 5.

The long-term cycling performance of periodic operation between NO/O_2/H_2O and H_2 was also studied by using the following sequence of step-gas switches:

(iv) He → 0.1 vol% NO/10 vol% O_2/5 vol% H_2O/1 vol% Kr/He (350 °C, 3 min) → 5 vol% H_2/He (350 °C, 1 min) → 0.1 vol% NO/10 vol% O_2/5 vol% H_2O/1 vol% Kr/He (350 °C, 3 min) → 5 vol% H_2/He (350 °C, 1 min) → repeat for 30 cycles. The step-gas switch NO/O_2/H_2O (3 min) → H_2 (1 min) was defined as one cycle.

The 3-min He purge appeared in (iii) served to remove practically all gases from the lines/micro-reactor before the switch to the H_2-containing gas stream for the correct analysis of the gas responses related only to the reduction kinetics of NO_x-s, and to minimize NO_x-s decomposition from the catalyst's surface. The effluent gas stream from the

outlet of micro-reactor was connected to an *on-line* mass spectrometer (Balzers, Omnistar, 1–300 amu) for gas analysis. The following mass numbers (m/z) were monitored: NH_3 (15), N_2 (28), NO (30), N_2O (44), NO_2 (46) and Kr (84). The MS signals were converted into concentration after using certified gas mixtures (1000 ppm NH_3/He, 1% N_2/He, 984 ppm NO/He, 144 ppm N_2O/He, and 180 ppm NO_2/1% O_2/He). The contributions of N_2O to $m/z = 28$ and NO_2 to $m/z = 30$ signal were considered.

During the catalyst treatment with the NO-containing feed gas stream, NO_x adsorbed species were formed (nitrites/nitrates). The latter could potentially react with H_2 to form N_2, N_2O and/or NH_3 during the step-gas switch to the H_2-containing feed gas stream. Prior to each transient experiment described in (i) or (ii), the sample (W = 50 mg) was ground and sieved in particles of less than 106 μm in size, reduced in 5 vol% H_2/He at 400 °C/1 h, and purged in He gas flow at 400 °C/10 min

2.4. Transient rates and amounts of NO_x adsorption and reaction products formation

The transient rate of NO consumption (R_{NO}) during the adsorption step in the step-gas switches (i) - (iv) was estimated using material balance, Eq. (2). The amount of NO consumed (mol g^{-1}) was estimated after integration of the rate vs time response curve.

$$R_{NO}(mol\ g^{-1}s^{-1}) = \frac{F_T}{W} y^f_{NO}(Z_{Kr}(t) - Z_{NO}(t)) \quad (2)$$

In Eq. (2), $Z_{Kr}(t)$ and $Z_{NO}(t)$ are the dimensionless concentrations of Kr tracer gas and NO, respectively, where $Z_i(t) = y_i(t)/y_i^f$. Here, $y_i(t)$ is the mole fraction of Kr or NO at a given time during the transient adsorption experiment, and yi^f is the mole fraction corresponding to the feed gas composition (1000 ppm for NO and 1 vol% for Kr). Thus, $Z_i = 1.0$ when the Kr or the NO signal in the mass spectrometer takes the corresponding value in the feed gas stream. The transient formation rate of product i, R_i (mol g^{-1} s^{-1}), e.g., NH_3, N_2, NO_2 or N_2O was estimated based on the material balance given by Eq. (3), where the accumulation term during the transient period was found negligible; the same was true in the case of applying Eq. (2).

$$R_i(mol\ g^{-1}s^{-1}) = \frac{F_T}{W}(y_i(t)) \quad (3)$$

The transient rate (mol g^{-1} s^{-1}) of adsorbed NO_x-s formation was estimated via the material balance described in Eq. (4), where the accumulation term with respect to NO(g) in the CSTR microreactor was found negligible.

$$R_{NO_x-s}(mol\ g^{-1}s^{-1}) = R_{NO} - (2R_{N_2} + 2R_{N_2O} + R_{NO_2}) \quad (4)$$

Integration of the transient rate response curves (Eqs. (3,4)) provides the amount (mol g^{-1}) of gaseous species and NO_x-s formed, respectively. The N_2-selectivity related to the sequence of step-gas switches (i) or (iii), and the NO_x-s conversion for the transient experiment (iii) are described in the Supporting Information (SI, Eqs. (S1)-(S3)).

3. Results and discussion

3.1. Characterization of catalysts

3.1.1. Pt loading and powder X-ray diffraction (XRD) analyses

The Pt loading in the synthesized Pt/$Co_1Mg_2Al_1O_x$-LDO catalyst was found to be 0.59 wt%. Powder X-ray diffractograms of $Co_1Mg_2Al_1O_x$-CO_3-LDH, Pt/$Co_1Mg_2Al_1O_x$-CO_3-LDH, $Co_1Mg_2Al_1O_x$-LDO and Pt/$Co_1Mg_2Al_1O_x$-LDO solids are presented in Fig. S1 (SI). Both $Co_1Mg_2Al_1O_x$-CO_3-LDH and Pt/$Co_1Mg_2Al_1O_x$-CO_3-LDH samples showed the typical layered structure of hydrotalcite [5,6,32]. After treatment in air at 500 °C/5 h, both LDH samples lost their intrinsic structure and had been converted into mixed metal oxides. The newly formed diffraction peaks confirmed the presence of Co_3O_4 (JCPDS No. 74–1656) and periclase MgO (JCPDS No. 77–2364). However, for both samples, no diffraction peaks belonging to γ-Al_2O_3, Pt or PtO_x phases were observed. The Pt metal phase was highly dispersed as evidenced by HAADF-STEM to be reported next. The Pt mean particle size was thus significantly smaller than the detection limit of powder XRD and the low Pt loading (0.59 wt%) used is also noted.

3.1.2. Scanning Transmission Electron Microscopy (STEM)

High-angle annular dark-field scanning transmission electron microscopy (HAADF-STEM) images and corresponding energy dispersive X-ray (EDX) analysis mapping of the fresh calcined (500 °C/5 h) Pt/$Co_1Mg_2Al_1O_x$-LDO sample are shown in Fig. 1 and Fig. S2 (SI). The EDX elemental mapping (Fig. S2A) reveals a homogeneous distribution of Co, Mg, Al, O and Pt elements in the sample. The well distributed Pt in atomic state and/or in very small PtO_x clusters (less than 0.5 nm) is evidenced (Fig. 1), consistent with the powder XRD results (Fig. S1). The STEM image shown in Fig. S2B reveals that Pt/$Co_1Mg_2Al_1O_x$-LDO has a "flower-like" type morphology [6].

The possibility of Pt particles agglomeration during the performed NO_x adsorption followed by H_2 reduction (see Section 3.3) was examined by HAADF-STEM images (Figs. S3 and S4) after repeating an oxidation (20% O_2, 350 °C/20 min) followed by reduction (5% H_2, 350 °C/10 min) cycle (aging process) six times. It is seen that Pt clusters were only slightly agglomerated after the aging applied. Some of the agglomerated Pt particles were found loosely packed (Fig. S4A), while others exhibited regular lattice arrangement (Fig. S4B) without forming larger Pt particles. The majority of Pt was found to be well distributed as very small clusters (below about 0.6 nm) according to Fig. S4C, suggesting a small only aggregation of Pt particles, in agreement with the H_2-TPD results obtained on the same aged catalyst (Section 3.1.4).

3.1.3. Texture analysis

The specific surface area (SSA), pore volume (V_p), and average pore size (d_p) of $Co_1Mg_2Al_1O_x$-LDO were found to be: 271 m^2 g^{-1}, 1.43 cm^3 g^{-1} and 21.2 nm, respectively. For the Pt/$Co_1Mg_2Al_1O_x$-LDO solid, only small alterations were found, namely: 295 m^2 g^{-1}, 1.34 cm^3 g^{-1} and 18.2 nm, respectively.

3.1.4. H_2 Temperature Programmed Desorption (H_2-TPD)

Fig. 2 A presents the H_2-TPD trace of the Pt/$Co_1Mg_2Al_1O_x$-LDO

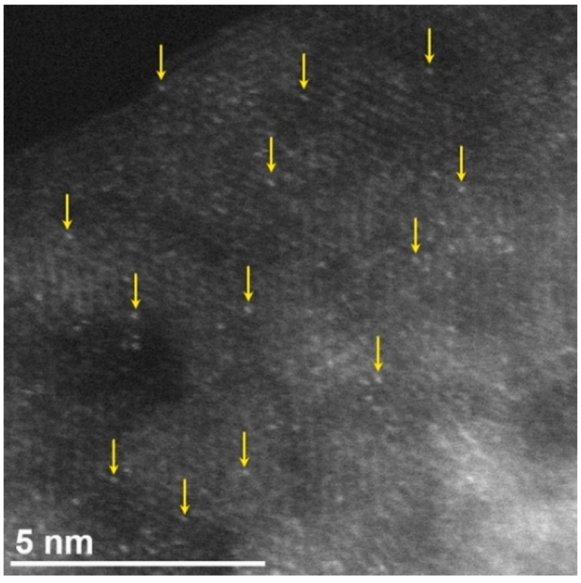

Fig. 1. HAADF-STEM image of Pt/$Co_1Mg_2Al_1O_x$-LDO solid. The white spots indicate Pt atoms and/or very small Pt clusters (less than 0.5 nm).

catalyst and that after deconvolution (Gaussian peak shape). The total amount of H_2 desorbed was used to estimate the dispersion of Pt (D_{Pt}, %) and a mean Pt particle size, d_{Pt} (nm) via Eq. (1). The dispersion of Pt was found to be 96% providing a mean Pt particle size of ~ 1.1 nm. This result is in line with the HAADF-STEM results (Fig. 1), where very small clusters of Pt (less than 1.0 nm) can be clearly seen. Based on an early pioneering work by Kip et al. [35] on the determination of Pt metal particle size in highly dispersed Pt catalysts using H_2 chemisorption, EXAFS and modeling studies, high H/M values (larger than unity) are justified when multiple hydrogen chemisorption (high H/M_s) occurs on edge and corner metal atoms in very small Pt nanoparticles. In the present H_2-TPD trace (Fig. 2A), an experimental value of H/M = 0.96 was estimated. However, a larger value might be considered since weakly chemisorbed atomic hydrogen and di-hydrogen [36] might had been desorbed at 30 °C (under the He gas flow) before the start of the TPD run. Thus, smaller than 1.1 nm in size Pt nanoparticles would be estimated as indeed observed by the direct HAADF-STEM measurements (Fig. 1).

The H_2-TPD trace (Fig. 2A) suggests strong heterogeneity for the present supported Pt surface (different E_{Pt-H} bond strengths). Five individual hydrogen desorption peaks were obtained after deconvolution (T_M = 110, 183, 261, 374 and 492 °C). The high temperature desorption peak at T_M = 492 °C might be linked to strongly adsorbed H-s arising from some electronic modifications of very small Pt nanoparticles in intimate contact with the support to form oxidized Pt^{2+} sites [37], and to some hydrogen spillover. The latter, however, is not the case as discussed in Section 2.2.1. This H_2 desorption peak (T_M = 492 °C) was found to correspond to the largest amount (7.7 μmol g_{cat}^{-1}), accounting for ~ 54% of the total amount, indicating that a large portion of H-s is strongly chemisorbed on the smaller in size Pt clusters. The four desorption peaks in the 50–450 °C range (Fig. 2A) is the result of several types of H-s formed on a rather narrow Pt cluster size distribution (e.g., edges of different facets, steps, corners, etc). The 1st peak (T_M = 110 °C) might be assigned to a weakly adsorbed H-s on Pt, and the 2nd, 3rd and 4th desorption peaks (T_M = 183, 261 and 374 °C, respectively) to irreversibly adsorbed H-s at 30 °C of higher binding strength, E_{Pt-H} [38,39]. An approximate distribution (percentage of total adsorbed H-s) of the five hydrogen adsorbed states (peaks (1)-(5); T_M= 110, 183, 261, 374 and 492 °C) was found to be: 18%, 10%, 5%, 13% and 54%, respectively. The H_2-TPD trace of the aged catalyst (see Section 3.1.2) is reported in Fig. S5 (SI). The total amount of desorbed H_2 was ~ 13.1 μmol g^{-1}, corresponding to ~ 87% dispersion and ~ 1.2 nm mean metal Pt particle size. This result shows that agglomeration and loss of surface Pt was small after the applied redox aging treatment in agreement with the HAADF-STEM results (Fig. 1, S3 and S4). The distribution in the binding strength of H-Pt_s, however, largely changed as evidenced by the peak shape and position of the H-binding states in the H_2-TPD traces of fresh and aged Pt/$Co_1Mg_2Al_1O_x$-LDO catalyst samples (after deconvolution).

In situ DRIFTS-CO chemisorption (2 vol% CO/He) experiments at 30 °C were conducted to characterize the Pt surface sites of the fresh and reduced Pt/$Co_1Mg_2Al_1O_x$-LDO catalyst sample, and results are shown in Fig. 2B. The recorded IR bands at 2174 and 2122 cm^{-1} are due to gaseous CO, whereas the high-frequency (HF) IR bands at 2060 and 2030 cm^{-1} (including a shoulder at ~ 1980 cm^{-1}) correspond to linear-types adsorbed CO on highly dispersed Pt (d_{Pt} < 1 nm). It was reported [40, 41] that on reduced Pt/metal oxide surfaces, Pt atoms and monoatomic Pt^o exist on flat surfaces, edges and kinks. The CO IR bands centered at 1935 and 1870 cm^{-1} are due to bridged-type (e.g., hollow site) CO adsorption on Pt [40,41]. These results are in line with the HAADF-STEM (Fig. 1) and H_2-TPD (Fig. 2A), where the five binding states of H-Pt_s identified are consistent to the multiple DRIFTS CO chemisorption states observed on very small (< 0.5 nm) and larger Pt clusters/nanoparticles.

3.2. Transient NO_x adsorption kinetic studies

A series of transient kinetic experiments were designed and performed over $Co_1Mg_2Al_1O_x$-LDO and Pt/$Co_1Mg_2Al_1O_x$-LDO samples to elucidate the dynamic kinetic behavior and important mechanistic steps of the NO_x storage process in the absence or presence of H_2O and CO_2 but also after presulfation of the catalyst with 20 or 50 ppm SO_2/He gas treatment at 350 °C. The following information was obtained:

(a) The dynamic evolution of NO consumption, NO_x adsorption, N_2, N_2O and NO_2 formation rates during the step-gas concentration switch He → 0.1% NO/10% O_2/x% H_2O and/or 7% CO_2/1% Kr/He (T, t) in the 200–400 °C range; x = 0 or 5.
(b) The amounts (μmol g^{-1}) of NO-cons, N_2, N_2O, NO_2 as well as of NO_x-s formed (NO_x storage capacity, NSC) after 20-min treatment of the catalyst in the 0.1% NO/10 vol% O_2/x% H_2O and/or 7% CO_2/1% Kr/He gas flow; x = 0 or 5.
(c) The dynamic evolution and amount (μmol g^{-1}) of NO_x-s (NSC) during the last switch of the following sequence of step-gas switches: 20 or 50 ppm SO_2/He (350 °C/20 min) → He (3 min) → 0.1% NO/10% O_2/He (350 °C/20 min).

3.2.1. Transient NO_x adsorption (NO/O_2/He)

The dynamic rate (μmol g^{-1} s^{-1}) profiles of NO-cons, NO_2 formation and NO_x-s adsorption obtained after the step-gas concentration switch He → 0.1% NO/10% O_2/1% Kr/He (T, t) over the Pt/$Co_1Mg_2Al_1O_x$-LDO catalyst at 200, 300 and 400 °C are shown in Fig. 3A-C. It should be emphasized that no N_2 or N_2O were detected, which suggests that NO decomposition did not occur at the applied reaction conditions.

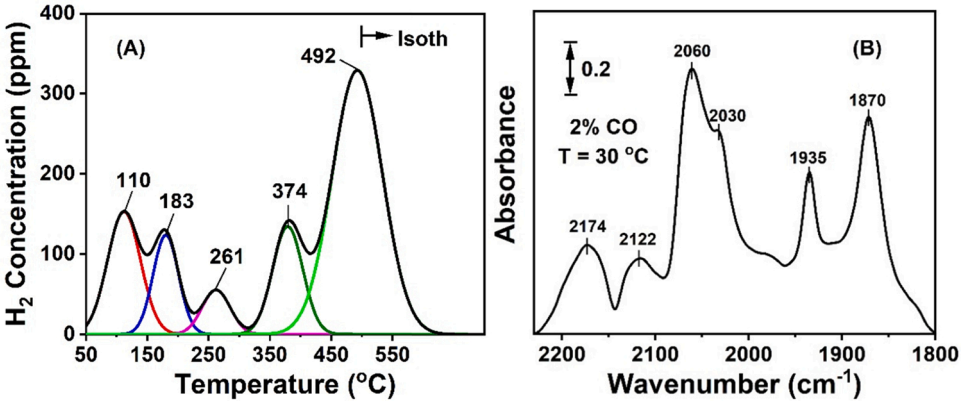

Fig. 2. (A) Deconvoluted (Gaussian peaks) H_2-TPD trace obtained on 0.59 wt% Pt/$Co_1Mg_2Al_1O_x$-LDO catalyst; F_{He} = 50 NmL min^{-1}; β = 30 °C min^{-1}; W = 0.3 g. (B) In-situ DRIFTS spectra recorded in the 2250–1800 cm^{-1} range over the Pt/$Co_1Mg_2Al_1O_x$-LDO sample (reduced) after 1 h in 2 vol% CO/He at 30 °C.

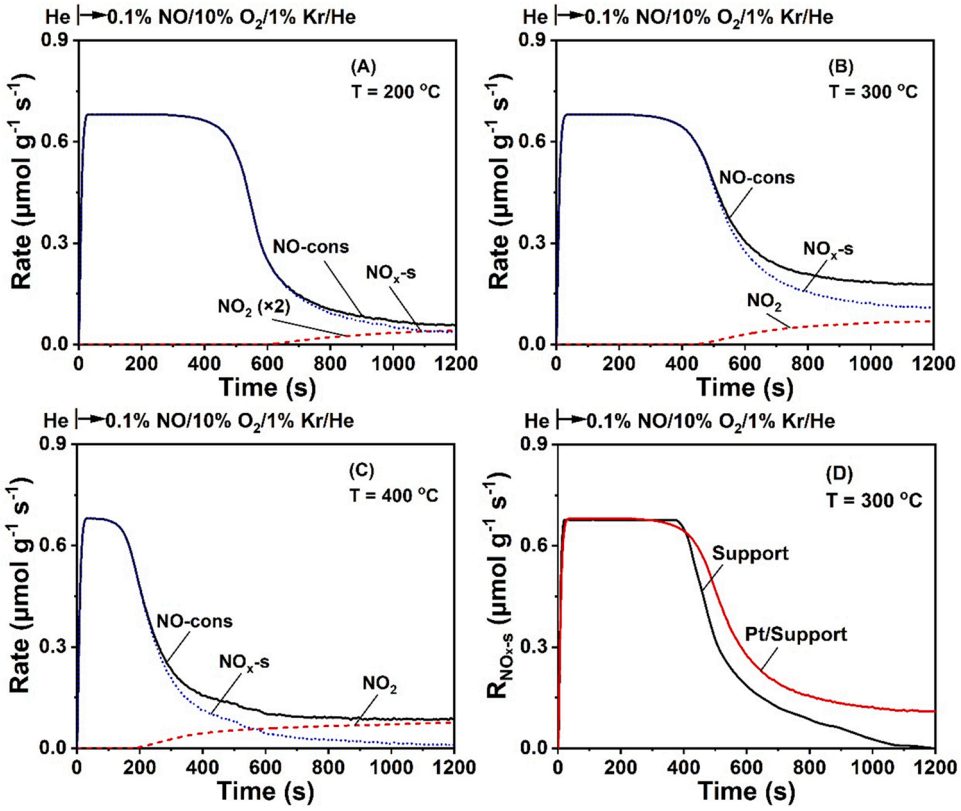

Fig. 3. Dynamic rate profiles (μmol g^{-1} s^{-1}) of NO-cons, NO_2 formation and NO_x-s at (A) 200 °C, (B) 300 °C and (C) 400 °C after the step-gas switch He → 0.1% NO/10% O_2/1% Kr/He (T, 20 min) over the $Pt/Co_1Mg_2Al_1O_x$-LDO catalyst. (D) Comparison of NO_x-s transient rates between the support and Pt/support samples; W = 50 mg; GHSV = 60,000 h^{-1}.

Moreover, the evolution rate of NO-cons was similar to that of NO_x-s at the low temperature of 200 °C, in agreement with the low NO_2 formation rate (Fig. 3A). By increasing the reaction temperature, the transient rate curves of NO-cons and NO_x-s do not follow closely each other after 450 and 200 s at 300 and 400 °C, respectively. At this point of time, NO_2 starts to form with increasing rate. The catalyst exhibits an obviously larger NO_2 formation rate at higher temperatures due to an enhanced NO oxidation (Fig. 3A-C).

The rate of NO_x chemisorption at 400 °C (Fig. 3C) drops quickly after ~ 200 s, and becomes practically zero after 20 min, as opposed to the case at 300 °C (Fig. 3B). A fast and complete NO consumption (chemisorption) is observed during the first 120 s of the transient after NO/O_2 was introduced in the reactor, regardless of the reaction temperature. This is equivalent to 100% NO_x adsorption efficiency. At 300 °C, a remarkable NO_x-s adsorption efficiency for ~ 7 min on reaction stream was obtained (Fig. 3B, NO-cons curve), as opposed to the higher T of 400 °C (Fig. 3C).

Similar in shape transient rate evolution curves of $R_{NOx\text{-}s}$ at 300 °C were observed between the LDO support alone and the supported Pt catalyst (Fig. 3**D**). Both solids exhibit significant NO_x-s adsorption efficiency for the first 5 min. After ~ 20 min in the NO/O_2 gas treatment, the $R_{NOx\text{-}s}$ for the support decreases to zero, while a tail is observed for the $Pt/Co_1Mg_2Al_1O_x$-LDO catalyst. It is noted that more NO_2 was formed on the support alone (Fig. S6), indicating that the extent of NO_x-s formation was reduced compared with that on the supported Pt catalyst.

Fig. 4 presents comparative amounts of NO-cons, NO_x-s, and NO_2(g) for the $Pt/Co_1Mg_2Al_1O_x$-LDO catalyst as a function of reaction temperature. The NO consumption and NO_x adsorption amounts pass through a maximum at 300 °C (NO-cons = 577.7 μmol g^{-1} and NO_x-s = 536.4 μmol g^{-1}), while the amount of NO_2(g) increases with reaction temperature; a value of 67.5 μmol g^{-1} was obtained at 400 °C. The amounts of NO-cons, NO_x-s and NO_2(g) at 300 °C over the $Co_1Mg_2Al_1O_x$-LDO support alone

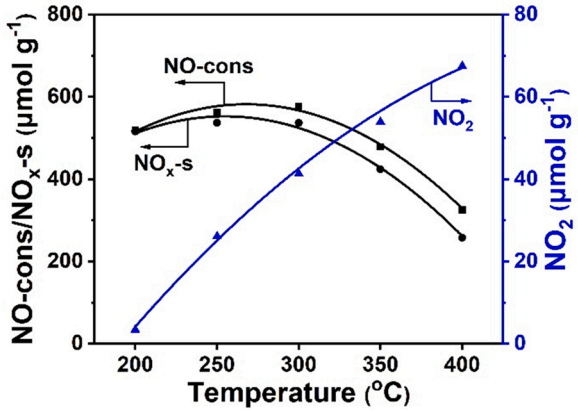

Fig. 4. Amounts (μmol g^{-1}) of NO consumed (NO-cons), NO_x chemisorbed (NO_x-s) and NO_2 formed (right) in the 200–400 °C range after the step-gas switch He → 0.1% NO/10% O_2/1% Kr/He (T, 20 min) over the $Pt/Co_1Mg_2Al_1O_x$-LDO catalyst; F_T = 50 NmL min^{-1}; W = 50 mg; GHSV = 60,000 h^{-1}.

were found to be 480.9, 418 and 62.9 μmol g^{-1}, respectively. A surface coverage of NO_x-s, θ_{NOx} ~ 17.9 was estimated for $Pt/Co_1Mg_2Al_1O_x$-LDO compared to the value of ~ 4.9 obtained when no oxygen was present in the NO feed gas stream.

Based on the results presented in Fig. 3D, both the $Co_1Mg_2Al_1O_x$-LDO support and the $Pt/Co_1Mg_2Al_1O_x$-LDO catalyst accommodate large amounts of chemisorbed NO_x at 300 °C when oxygen is present in the NO feed gas stream, named NO_x storage capacity (NSC). The NSC of support alone at 300 °C is ~ 78% of that on the supported Pt solid. The presence of Pt is to enhance the oxidation rate of NO to NO_2, the adsorption of which is energetically favorable on support's sites. There is

no evidence from this work that Pt-support interfacial sites may contribute to a greater extent to the NSC or the rate of NO_2 formation. It is noted that if all loaded Pt (0.59 wt%) were in the form of atomic Pt on the surface of support, this would correspond to about 30 μmol/g_{cat} of surface Pt. This number is about four times lower than the difference in the NSC between $Pt/Co_1Mg_2Al_1O_x$-LDO and the support.

The NSR approach for NO_x reduction has been developed for lean-burn engines (mobile applications) using initially the $Pt/BaO/Al_2O_3$ NSR catalytic system [2,3]. Since no such approach was used for stationary NO_x control applications, the NO_x storage capacity (NSC) of the present $Pt/Co_1Mg_2Al_1O_x$-LDO catalytic system could be only compared with those reported for mobile applications and results are provided in Table 1 for various NO-containing gas compositions that include H_2O and/or CO_2 (see Section 3.2.2). The present 0.59 wt% $Pt/Co_1Mg_2Al_1O_x$-LDO catalyst outperforms the NSC values reported on those of Ba/Al_2O_3-based supported Pt solids used in LNT mobile applications. The following are noted: (i) no BaO as NO_x storage component is used in the $Pt/Co_1Mg_2Al_1O_x$-LDO solid, (ii) Pt loading (0.59 wt%) is lower than that used in other catalytic systems (at least 1.0 wt%), and (iii) NSC was estimated over a period of 20 min (Fig. 3), thus, a higher NSC value at saturation should be expected.

Table 1
Comparison of NO_x storage capacity (NSC) reported in the literature on $Pt/BaO-Al_2O_3$ based NO_x adsorbents with the current $Co_1Mg_2Al_1O_x$ and $Pt/Co_1Mg_2Al_1O_x$ solids at 300 °C.

NSR Catalyst	NSC (μmol g^{-1})	Gas mixture	GHSV	Reference
$Co_1Mg_2Al_1O_x$	418	1000 ppm NO/ 10% O_2	60,000 h^{-1}	This work
0.59Pt/ $Co_1Mg_2Al_1O_x$	536	1000 ppm NO/ 10% O_2		
	337	1000 ppm NO/ 10% O_2/7% CO_2		
	290	1000 ppm NO/ 10% O_2/5% H_2O		
	234	1000 ppm NO/ 10% O_2/7% CO_2/ 5% H_2O		
1.5Pt/15Ba/ Al_2O_3	267	380 ppm NO/5% O_2	30,000 h^{-1}	[42]
1.5Pt/15Ba/ Al_2O_3-R	306			
1.5Pt/7.6Fe/ 15Ba/Al_2O_3	245			
1.5Pt/7.6Fe/ 15Ba/Al_2O_3-R	239			
1Pt/10Ba/Al_2O_3	167	500 ppm NO/8% O_2	48,000 mL g^{-1} h^{-1}	[43]
	159	500 ppm NO/8% O_2/2% CO_2/2% H_2O		
1Pt/20Ba/Al_2O_3	319	500 ppm NO/5% O_2	100,000 h^{-1}	[44]
1Pt/16BaO/ Al_2O_3	292	500 ppm NO_2/5% O_2	12,000 h^{-1}	[45]
	346	900 ppm NO_2/5% O2		
	183	500 ppm/NO_2/5% CO_2		
	278	900 ppm/NO_2/5% CO_2		
1Pt/20Ba/Al_2O_3	581	1000 ppm NO/3% O_2	99,900 mL g^{-1} h^{-1}	[46]
0.5Pt/15Ba/ Al_2O_3	220	1000 ppm NO/ 10% O_2	40,000 mL g^{-1} h^{-1}	[47]
1Pt/15Ba/Al_2O_3	270			
0.5Pt/10CoO_x/ 15Ba/Al_2O_3	410			
1Pt/30Ba/Al_2O_3	1112	2000 ppm NO/4% O_2	29,000 mL g^{-1} h^{-1}	[48]
	828	2000 ppm NO/4% O_2/10% CO_2		
	474	2000 ppm NO/4% O_2/10% CO_2/10% H_2O		

Fig. 5 A shows comparative transient kinetic rate profiles of adsorbed NO_x-s at 300 °C in the absence (curve a) and presence (curve b) of gaseous oxygen in the NO adsorption gas mixture, while Fig. 5B shows respective amounts of NO_x-s (μmol g^{-1}) in the 200–400 °C range for the $Pt/Co_1Mg_2Al_1O_x$-LDO catalyst. Although similar amounts of NO-cons were obtained regardless of the absence or presence of O_2, the adsorption rates and amounts of NO_x-s are largely different. In the presence of O_2, the catalyst exhibits an initial rate of NO_x chemisorption ~ 2.5 times larger and with longer plateau than in the absence of oxygen in the NO feed gas stream (Fig. 5A). Moreover, a very high NO_x adsorption capacity over the entire 200–400 °C range was obtained when O_2 was present in the NO feed gas stream (Fig. 5B, curve b).

3.2.2. *Effect of H_2O and CO_2 on the transient NO_x adsorption kinetics*

Many research works have shown that LDOs have relatively good CO_2 adsorption capacity, particularly in the 200–400 °C range [49]. Therefore, it is reasonably expected that the presence of CO_2 in the NO-containing feed gas stream will compete for NO_x adsorption sites. Besides, water vapor is present in flue gas streams, and this should also be considered in studying its influence on NO_x adsorption and oxidation of NO to NO_2 [6,50]. For most stationary NO_x control applications (use of NH_3-SCR), the concentrations of CO_2 and H_2O are in the range of 2–10 vol% [8,51,52]. Thus, during the periodic operation between $NO/O_2/CO_2/H_2O$ and H_2, 5 vol% H_2O and 7 vol% CO_2 were used for the NO_x adsorption step on the present Pt/LDO catalytic system.

Fig. 6 A and B show comparative transient rates of NO_x-s chemisorption in the presence of 5 vol% H_2O and/or 7 vol% CO_2 at 200 and 400 °C, respectively. At 200 °C (Fig. 6A), a long plateau (~ 450 s) of complete NO_x chemisorption was obtained in the absence of H_2O and CO_2, while in the presence of H_2O or CO_2, the extent of plateau was largely decreased to ~ 100 s. When H_2O and CO_2 were co-fed in the NO/O_2/He feed gas stream, no plateau was observed.

Although a similar NO_x chemisorption plateau was observed in the presence of H_2O or CO_2 (Fig. 6A), the effect of H_2O was more pronounced leading to a faster decrease in the transient rate of NO_x-s following the plateau compared with the case of CO_2. It appears also that the co-presence of H_2O and CO_2 largely deteriorates the NO_x-s performance of the solid.

At the higher temperature of 400 °C (Fig. 6B), regardless of the composition of the NO_x feed gas stream, a significantly smaller extent in time of the plateau (maximum rate of NO_x-s) was obtained. This behavior must be related to the reduced thermal stability of adsorbed NO_x-s formed on both the Pt and the support surfaces. In addition, the influence of H_2O and CO_2 on NO_x chemisorption changes remarkably compared to that at 200 °C (Fig. 6A). In the latter case, the co-presence of CO_2 and H_2O led to the worst NO_x chemisorption performance as opposed to the case of 400 °C (Fig. 6B).

Fig. 6 C presents the effect of H_2O and/or CO_2 on the amount of NO_x-s (NSC) on the $Pt/Co_1Mg_2Al_1O_x$-LDO catalyst in the 200–400 °C range estimated after 20 min in both the $0.1\%NO/10\%O_2$/He, and $0.1\%NO/10\%O_2/5\%H_2O$ and/or $7\%CO_2$/He gas treatments. At 200 °C, when CO_2 or H_2O was present, the amount of NO_x-s was 382.9 and 234.4 μmol g^{-1}, respectively. The co-presence of H_2O and CO_2 led to a further reduction in NO_x-s, ca. 114.7 μmol g^{-1}. In the absence of H_2O and CO_2, the amount of NO_x-s was 515.6 μmol g^{-1}. Thus, 25.7%, 54.5% and 77.8% reduction in NSC was noticed in the presence of 7 vol% CO_2, 5 vol% H_2O, and when both CO_2 and H_2O were present, respectively. It should be noted that the negative impact of H_2O on NO_x-s at 200 °C is twice as that of CO_2. At 400 °C, the presence of H_2O increased the NSC by 14.6% but that of CO_2 caused a negative effect (21% reduction in NO_x-s). On the other hand, the co-presence of H_2O and CO_2 had no practical effect on the NSC. Regardless of the reaction temperature, the negative impact of CO_2 on the rate and amount of adsorbed NO_x is due to the high stability

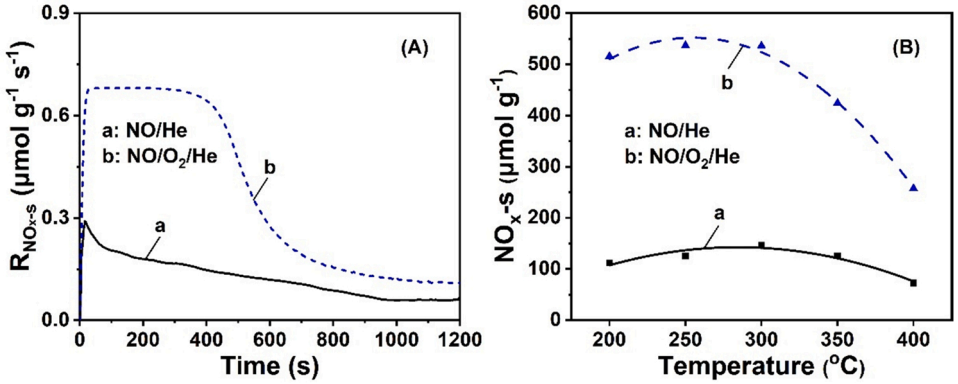

Fig. 5. (A) Dynamic rate profiles (μmol g^{-1} s^{-1}) of NO_x chemisorbed at 300 °C and (B) amounts of NO_x chemisorbed in the 200–400 °C range following the step-gas switches: (a) He → 0.1% NO/1% Kr/He (T, 20 min), and (b) He → 0.1% NO/10% O_2/1% Ar/He (T, 20 min) over the Pt/$Co_1Mg_2Al_1O_x$-LDO catalyst. F_T = 50 N mL min^{-1}; W = 50 mg; GHSV = 60,000 h^{-1}.

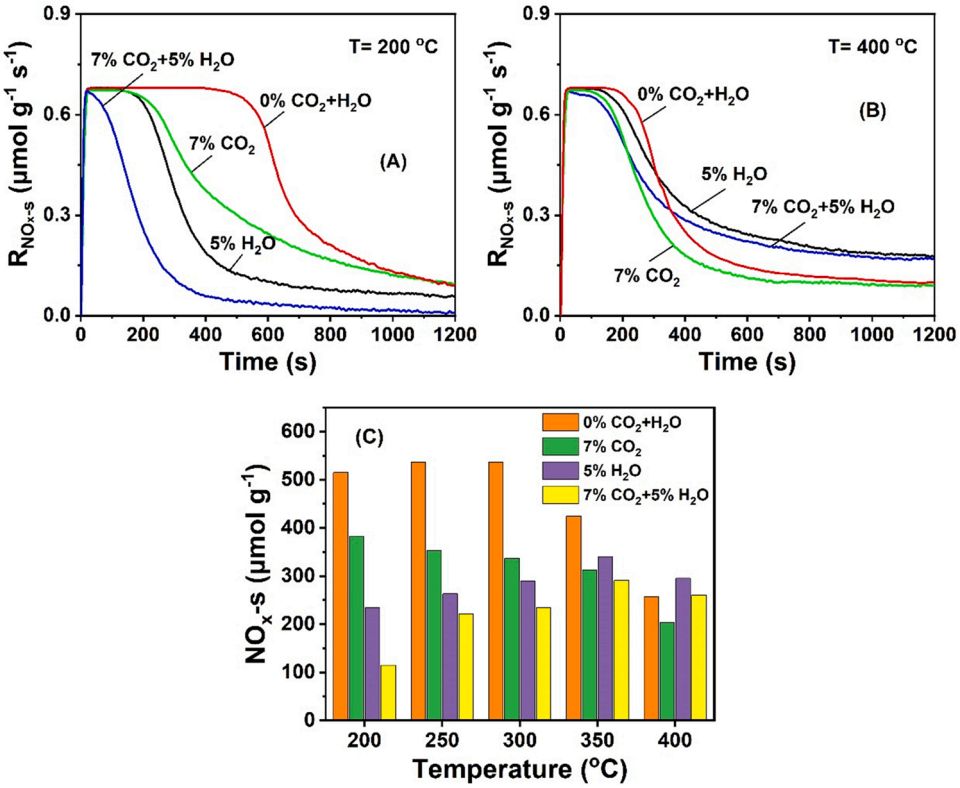

Fig. 6. Transient rate profiles (μmol g^{-1} s^{-1}) of NO_x-s at (A) 200 °C and (B) 400 °C after the switch He → 0.1% NO/10% O_2/1% Kr/He (T, 20 min) in the presence of H_2O and/or CO_2 over the Pt/$Co_1Mg_2Al_1O_x$-LDO catalyst. (C) Amounts (μmol g^{-1}) of NO_x-s obtained at 200–400 °C following the step-gas switch He → 0.1% NO/10% O_2/5%H_2O and/or 7%CO_2/1%Kr/He (T, 20 min). F_T = 50 NmL min^{-1}; W= 50 mg; GHSV= 60,000 h^{-1}.

of the formed carbonates relative to the nitrate species [53]. At 200 °C, H_2O dissociation on surface Pt sites significantly reduced the rate of NO oxidation, resulting eventually to a decrease in the rate and amount of adsorbed NO_x-s (Fig. 6A, C) [6,48]. This prohibiting effect at 200 °C appears to be very weak at 400 °C due to the good NO oxidation activity of Co_3O_4.

Based on the transient response curves of CO_2 recorded in the transient experiments of Fig. 6A, B (not reported), the amount of chemisorbed CO_2 was estimated. At 200 °C, when only CO_2 was present in the NO/O_2/He feed gas stream, CO_2 chemisorption was 179.5 μmol g^{-1}, accounting for 34.8% of the NO_x-s obtained in the absence of H_2O and CO_2 (515.6 μmol g^{-1}). However, the presence of CO_2 led only to a 25.7% reduction in NO_x-s, which indicates that chemisorption sites of NO_x and CO_2 on the present catalytic surface must be different. When H_2O and CO_2 were co-fed, the amount of chemisorbed CO_2 increased by 43% (256.6 μmol g^{-1}), which might be due to the formation of bicarbonate with the assistance of H_2O. Similar results were observed in the 250–400 °C range, suggesting that part of chemisorption sites for NO_x and CO_2 are not the same in nature. This result explains the good NSC poisoning resistance to CO_2 of the Pt/$Co_1Mg_2Al_1O_x$-LDO.

3.2.3. *NO_x storage capacity (NSC)*

As illustrated in Fig. 3, the transient rate curves of NO_x-s and NO-cons were similar before the appearance of NO_2(g). After the reaction temperature was increased, NO_2 formation appeared earlier, and the rate of NO_x-s decreased significantly. The decomposition of adsorbed

NO_x-s into NO_2(g) is thus promoted with increasing reaction temperature. A maximum amount of NO_x-s was obtained at 300 °C, larger by ~ 3.7 times compared to the 0.1%NO/He gas treatment. The largest amounts of NO_x-s adsorption (536.4 μmol g^{-1}) obtained at 300 °C dictate an optimal temperature for NO_x storage (see Fig. 4). For the support alone, the amounts of NO_x-s become significant. When the temperature is higher than 300 °C, a large difference was observed in the amount of NO-cons (Fig. 4), which was caused by the enhanced rate in the thermal decomposition of adsorbed NO_x-s and NO reaction as well. The remarkable differences obtained in the transient kinetic rate of NO_x-s adsorption and the amount of NO_x-s formed between NO/He and NO/O_2/He gas treatments (Fig. 5) confirms the strong influence of O_2 on the NO chemical interaction paths with the surface of Pt/$Co_1Mg_2Al_1O_x$-LDO, to be discussed in the following Section 3.2.6.

3.2.4. Effect of SO_2 on the transient NO_x adsorption kinetics

Sulfur dioxide is known to cause strong deactivation of NO_x adsorbent materials [2,7,30]. Thus, the presence of SO_2 in the NO_x-containing flue gas stream (20 or 50 ppm) was evaluated. This study involved pretreatment of the catalyst in 20 or 50 ppm SO_2/He gas stream at 350 °C/20 min followed by He purge (3 min) and 0.1%NO/10%O_2/He gas treatment (350 °C/20 min). Obviously, the pre-sulfated catalyst resulted in reduced NO_x adsorption rates and amounts, where pre-treatment of the catalyst with 20 ppm SO_2 had less effect on the NSC (Fig. 7). A decrease in the amount of NO_x-s by 6.2% and 16.3% was seen after 20 min of NO/O_2/He gas treatment, following 20 or 50 ppm SO_2/He gas pretreatment, respectively. At the end of 20-min NO/O_2/He gas treatment, the catalyst was purged in He for 3 min and then reduced in 5% H_2/He for 10 min at 350 °C. At this point, a new cycle consisting of SO_2 pretreatment → He purge → NO gas treatment → He purge → H_2 reduction was repeated for 11 additional times, and results are provided in Fig. S7 (SI). It is rather clear that after 4 h in total gas pretreatment of Pt/LDO with 50 ppm SO_2/He, a very stable catalytic activity in terms of NSC was obtained (Fig. S7B).

In the absence of SO_2, a maximum NO_x-s adsorption rate lasted for ~ 5 min on reaction stream (curve 0), as opposed to the pre-sulfated catalyst (curves 1–6 refer to the corresponding cycle). After 6 cycles of SO_2 pretreatment, $R_{NOx\text{-}s}$ starts to decline very shortly following introduction of NO/O_2/He over the Pt/LDO catalyst (Fig. S7A), NO_x-s adsorption capacity (Fig. S7B) becomes lower but the catalyst shows stable NO_x-s reduction performance (see Section 3.3.4). There were practically no differences in $R_{NOx\text{-}s}$ over the last 6 cycles (not shown). During the SO_2 pretreatment stage, no SO_2 MS-signal was detected at the outlet of the reactor, indicating that all the introduced SO_2 was completely adsorbed. Based on this, a maximum value of ~ 7.9 mg S/g_{cat} can be reported after six cycles of SO_2 pretreatment-NO_x adsorption-NO_x reduction.

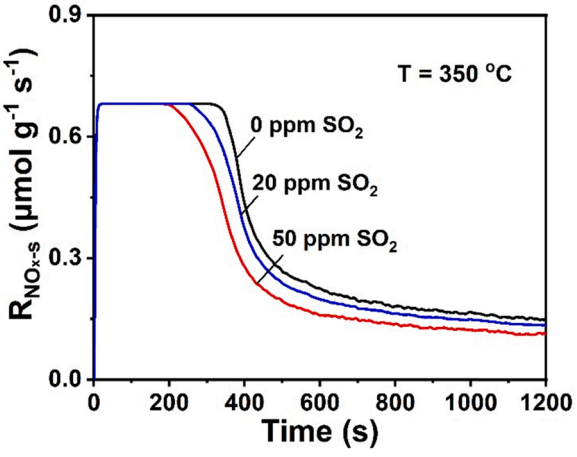

Fig. 7. Transient rate evolution profiles (μmol g^{-1} s^{-1}) of NO_x-s on the pre-sulfated Pt/$Co_1Mg_2Al_1O_x$-LDO catalyst; F_T = 50 NmL min^{-1}; W= 50 mg; GHSV= 60,000 h^{-1}.

3.2.5. Effect of catalyst pre-oxidation on the transient NO_x adsorption kinetics

For practical NO_x control applications of the present NSR process (Scheme 1), the consumption of hydrogen is a concern. The ideal scenario would be that the two "swing reactors" will not require a *fully reduced Pt* surface at the start of NO_x-adsorption process step. Thus, after the end of the short NO_x-reduction step by hydrogen (Scheme 1c), the catalyst could be kept *in air* before the next NO_x-adsorption process step (Scheme 1b). Fig. S8 (SI) compares the effect of catalyst pre-treatment, namely, H_2 reduction (pure H_2, 400 °C/1 h) versus calcination (20% O_2/He, 400 °C/1 h) on the NO_x-s transient rate response curves at 350 °C of the Pt/$Co_1Mg_2Al_1O_x$-LDO catalyst using the 0.1%NO/10%O_2/5%H_2O/He feed gas stream. It is illustrated that practically no differences in the transient NO_x-s adsorption behavior between pre-reduction and pre-oxidation of the catalyst occurred.

The remarkable behavior of the present catalytic system being able to provide a NSC independent of the initial oxidation state of Pt can be understood based on the following. In the case of pre-reduced Pt, NO oxidation proceeds easily, where reduced Pt sites are offered for dissociative oxygen adsorption (Pt-O). The latter species react with adsorbed NO (Pt-NO) to form NO_2(g), which in turn is chemisorbed on suitable support's sites (see following Section 3.2.6). In the case of oxidized Pt surface sites (Pt^{2+}), chemisorption of NO does also occur in the form of nitrosyl complexes, and these appear less thermally stable than on Pt^0 [41]. Given the fact that some surface reconstruction on the present small Pt clusters/nanoparticles was evidenced (see Section 3.1.2), it appears that the ~ 22% contribution of Pt to the NSC of supported Pt (Table 1) is sustainable, irrespective of the initial surface Pt oxidation state.

3.2.6. Mechanistic aspects of NO_x adsorption - The role of Pt metal

Based on earlier studies [54–56], a well-accepted mechanism of the NO interaction with Pt surfaces in the presence of excess gaseous oxygen can be described by the following elementary steps (5)-(12). Apparently, in the present work the N_2/N_2O formation rates were suppressed (Fig. 3) as opposed to the NO/He reaction (Fig. S9).

$$NO(g) + Pt \leftrightarrow NO\text{-}Pt \quad (5)$$

$$O_2(g) + 2\ Pt \rightarrow 2\ O\text{-}Pt \quad (6)$$

$$NO\text{-}Pt + Pt \rightarrow N\text{-}Pt + O\text{-}Pt \quad (7)$$

$$N\text{-}Pt + N\text{-}Pt \rightarrow N_2(g) + 2\ Pt \quad (8)$$

$$N\text{-}Pt + NO\text{-}Pt \rightarrow N_2O(g) + 2\ Pt \quad (9)$$

$$NO\text{-}Pt + NO\text{-}Pt \rightarrow N_2O(g) + O\text{-}Pt + Pt \quad (10)$$

$$NO\text{-}Pt + O\text{-}Pt \rightarrow NO_2\text{-}Pt + Pt \quad (11)$$

$$NO_2\text{-}Pt \leftrightarrow NO_2(g) + Pt \quad (12)$$

The fact that the support alone adsorbs an amount of NO_x-s significantly larger than one equivalent monolayer of Pt (~ 28.5 μmol NO g^{-1}) after 20 min of treatment in 0.1%NO/10%O_2/He at 300 °C, proves that the LDO support offers NO_x adsorption sites for nitrite and/or nitrate formation according to the elementary steps (13)-(14):

$$NO(g) \text{ or } NO_2(g) + s\text{-}O \leftrightarrow s\text{-}NO_2 \text{ or } s\text{-}NO_3 \quad (13)$$

$$O\text{-}Pt + s\text{-}NO_2 \leftrightarrow Pt + s\text{-}NO_3 \text{ (s: support site)} \quad (14)$$

For NSR catalysts, the oxidation of NO to NO_2 is an important step in storing NO_x species since the heat of adsorption of NO_2 is larger than that of NO [2]. In the absence of O_2, NO oxidation to NO_2 occurs on Pt through elementary steps (11)-(12), where surface oxygen originates

from the NO decomposition step. However, no NO_2 was detected upon the step-gas switch He → 0.1%NO/He (T, t) due either to its very small reaction rate or to the formation of strongly adsorbed nitrate species on the support and Pt in an irreversible manner (Eqs. (11) and (14)). With the increase of reaction temperature, the Pt surface can be partially re-generated (Eqs. (11)-(12)). Although Co_3O_4 has an excellent oxidation activity, it is not active towards NO decomposition [14,15]. The significant increase of NO_x adsorption in the presence of O_2 (Figs. 3 and 5) compared with the absence of O_2 (NO/He gas treatment, Fig. S9), partly reflects the enhancement of catalyst's NO oxidation ability towards the formation of thermally stable NO_x-s species (Fig. 5B). This is due to the presence of Co_3O_4 and MgO phases in the support, in addition to the presence of small Pt clusters/nanoparticles, which accelerate oxidation of NO to NO_2 [57]. The observed similar evolution of the rate response curves of NO-cons and NO_x-s at 200 °C (Fig. 3A) suggests that NO_2(g) was completely adsorbed on the support, according to reaction steps (13)-(14). After increasing the reaction temperature to 300 and 400 °C, the delay in the appearance of NO_2(g) is due to the decomposition of NO_x-s (Fig. 3B, C). Similarly, the LDO support alone has shown significant NO_x-s adsorption capacity (NSC) due to the presence of Co_3O_4 and MgO able to accommodate stable nitrite/nitrate species, largely independent of the presence of Pt (Table 1, Fig. 3D).

3.3. Transient NO_x-s reduction by hydrogen

The dynamic evolution of NO, N_2 and N_2O formation rates and their amounts (μmol g^{-1}) during isothermal reduction of pre-adsorbed NO_x by H_2 (NO_x reduction kinetics) in the 200–400 °C range was investigated both in the absence and presence of water and/or carbon dioxide, following the sequence of step-gas concentration switches: 0.1% NO/10% O_2/x% H_2O/1% Kr/He (T, 20 min) → He (T, 3 min) → 5% H_2/x% H_2O and/or 7% CO_2/He (T, t); x = 0 or 5.

3.3.1. Effect of H_2O

Fig. 8 shows the dynamic rate (μmol g^{-1} s^{-1}) evolution profiles of NO (A), N_2 (B) and N_2O (C) formation obtained during the transient NO_x reduction step at 350 °C with no or 5 vol% H_2O in the H_2-containing feed gas stream. Before the NO_x reduction step, the $Pt/Co_1Mg_2Al_1O_x$-LDO was treated in 0.1%NO/10%O_2/5% H_2O/He at 350 °C/20 min, followed by 3-min He purge. N_2 was the main reaction product of NO_x-s reduction by hydrogen with a small transient rate of N_2O (Fig. 8C) but larger NO formation rate; it is noted that R_{N2} is twice that of R_{NO} in terms

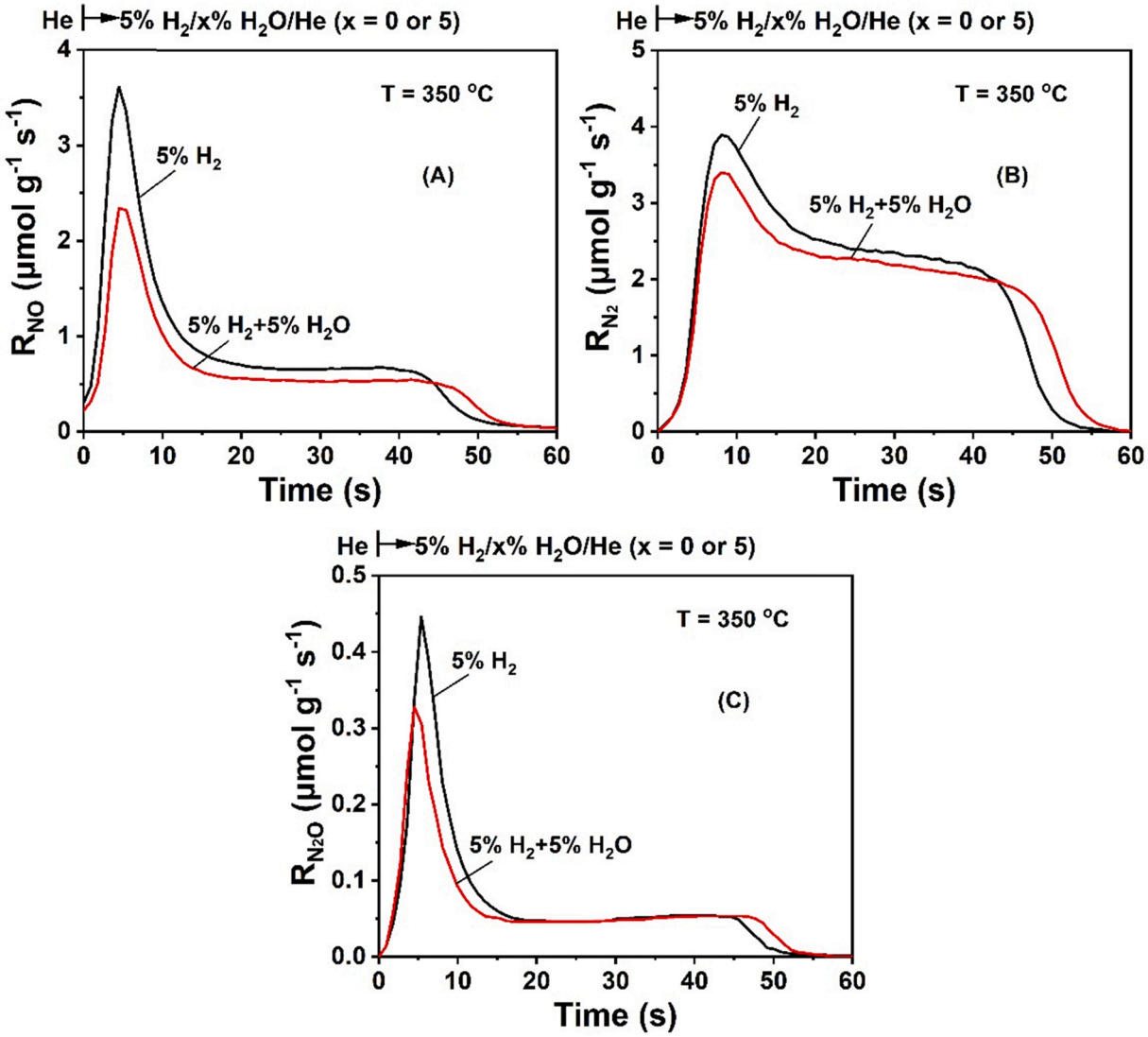

Fig. 8. Dynamic rate (μmol g^{-1} s^{-1}) evolution response curves of NO (A), N_2 (B) and N_2O (C) formation obtained at 350 °C during NO_x-reduction step according to the step-gas switches: 0.1% NO/10% O_2/5% H_2O/1% Kr/He (20 min) → He (3 min) → 5% H_2/x% H_2O/He (t) (x = 0 or 5) over the $Pt/Co_1Mg_2Al_1O_x$-LDO catalyst. F_T = 50 NmL min^{-1}; W = 50 mg; GHSV = 60,000 h^{-1}.

of NO_x-s reduction rate. The transient rate response of NO is due to the decomposition of nitrites/nitrates formed during the NO_x adsorption step. It is shown that the transient reduction of NO_x by 5 vol% H_2/He is practically complete after ~ 60 s, and this practically corresponds to the regeneration of the NO_x adsorption (storage) sites. It should be noted that no NH_3 was detected by mass spectrometry, indicating that NO and N_2O are the only by-products. The presence of 5% H_2O in the 5% H_2/He gas stream resulted in slightly lower rates of products formation and similar regeneration time. Related results obtained at 300 and 400 °C are given in Fig. S10A-C and Fig. S11A-C, respectively.

It is seen that the shapes of the transient response curves of NO, N_2 and N_2O formation rates are largely affected by the reaction temperature. A broad peak with a small shoulder was observed at 300 °C, as opposed to a sharp peak at 350 °C followed by a flat tail before vanishing. At higher temperatures (ca. 400 °C), a second peak under hydrogen reduction is observed for N_2/N_2O formation (Fig. S11B, C). The maximum rate of NO formation decreases with increasing reaction temperature, which is similar for the rate maximum of N_2 formation (compare Fig. 8, S10 and S11). The step-gas switch 0.1% NO/10% O_2/5% H_2O/1% Kr/He (20 min) → He (3 min) → 5% H_2O/He (t) was also performed at 350 °C (not presented), where only NO(g) was observed. This result suggests that possible contribution of water to the reduction of NO_x-s via H-s/OH-s formation must be excluded.

The formation of NO(g) under the 5%H_2/5%H_2O/He reduction conditions is related to the decomposition of adsorbed NO_x-s formed on both the Pt and support surfaces according to the results obtained for the support alone at 300 °C (Fig. S12). The gradual decrease of R_{NO} with reaction temperature observed on Pt/$Co_1Mg_2Al_1O_x$-LDO was mainly caused by the increase in the rate of reduction of NO_x-s with reaction T, and to a lesser extent by the loss of some NO_x-s desorbed during the 3-min He purge.

The NO(g), N_2(g) and N_2O(g) transient rate response curves recorded at 350 °C (Fig. 8) show a sharp peak at t ~ 5–8 s after the switch to the H_2/H_2O gas mixture, followed by an approximately constant rate period of ~ 25–30 s, followed by a quick drop to zero. These features are related to the dynamic kinetics of the reduction process of stored NO_x-s by hydrogen. The similar initial rate of NO_x-s decomposition into NO(g) at 300 °C (Fig. 8A) compared to the transient rate of NO_x-s reduction to N_2 (Fig. 8B) may suggest that decomposition of NO_x-s from the support sites to form NO(g) is followed by readsorption and reduction steps on the Pt surface. This reaction route may not be excluded. However, after careful inspection of both $R_{NO}(t)$ and $R_{N2}(t)$ at 300 °C (Fig. S10A and B) in the *first 15 s* of the transient reveals that N_2 formation rate is significantly lower than that of NO formation, thus largely excluding readsorption of NO followed by reduction under the 5%H_2/5%H_2O/He reaction conditions. The fact that reduction by hydrogen of stored NO_x-s on the support alone (Table S1, Fig. S12) proceeds with significantly lower rates than on Pt/LDO (Fig. S10), a different reaction path must be invoked to describe the NO_x-s reduction by hydrogen on the support. Efstathiou and his group [7,17,58] provided strong experimental evidence that adsorbed H-s on Pt diffuses towards NO_x-s adsorption sites on the MgO and CeO_2 supports during H_2-SCR on Pt/CeO_2-MgO and Pd/CeO_2 catalytic systems. The latter was probed after studying the effect of metal Pt particle size on the reduction rate of NO_x-s formed on the support as revealed by transient isotopic and DRIFTS studies.

According to the transient rate profile of NO(g) for the support alone (Fig. S12), the 1st sharp N_2(g) peak at 350 °C (t ~ 8 s, Fig. 8B) is due to the most active NO_x-s formed on the Pt surface (see Section 3.4, DRIFTS work), whereas the rest of the transient R_{N2} profile is due to the selective reduction of at least one additional but less active NO_x-s formed on the support. In an earlier study [59], a similar experiment conducted on Pt/Ba-Al_2O_3 NSR catalyst led the authors to conclude that reduction of NO_x by hydrogen was active at temperatures significantly lower than that of NO_x thermal decomposition, thus no themal release of stored NO_x is required, in agreement with the results of the present work.

In the TIH experiments reported in Fig. 8 and Figs. S10-S12, hydrogen dissociation occurs on the surface of Pt^0 to form H-s, able to reduce adsorbed NO_x. After the NO/O_2/H_2O/He (T, 20 min) gas treatment, Pt is likely to be partially oxidized. When the feed gas is switched to 5% H_2/5% H_2O/He in the 300–400 °C range, PtO_x reduction does occur, and θ_H is expected to increase with time in the H_2-containing feed gas stream. This is likely to have an influence on the transient kinetics of NO_x-s reduction to N_2/N_2O (shape of the transient response curve) with reaction temperature. A hydrogen-assisted NO dissociation mechanism was reported [60] with the activation energy of the N-O bond dissociation step (Eq. (10)) to be higher than that of H-assisted N-O dissociation step described by Eq. (15):

$$\text{NO-Pt} + \text{H-Pt} \rightarrow \text{N-Pt} + \text{OH-Pt} \quad (15)$$

The formed nitrogen adatoms can also participate in the formation of N_2O through Eq. (9) [23]. The fact that the formation of N_2 and N_2O via a hydrogen-assisted NO reduction mechanism proceeds with a lower activation energy than the recombination of two adsorbed atomic N to form N_2(g) might explain the earlier appearance of the first N_2 peak at T ≥ 350 °C, where oxidized Pt is rapidly get reduced by hydrogen, thus further promoting reaction step (15).

The H_2 concentration (Fig. S13A) and H_2O concentration (Fig. S13B) evolution response curves during the NO_x-s reduction step were also recorded. It is seen that no H_2 gas signal was detected during the first 50 s of the TIH step at 350–400 °C. This illustrates the larger reduction rates with increasing temperature, which are also influenced by the surface concentration of NO_x-s formed. The H_2 conversion (%) in the TIH step (Fig. S13A, 50 s) was estimated and results are presented in Fig. S14. H_2 conversion values higher than 90% were obtained in the 300–400 °C range, corresponding to complete regeneration of the catalyst. The H_2O concentration response curves revealed that a large amount of H_2O (11.6–10.6 mmol g^{-1}) was adsorbed on the catalyst surface (300–400 °C), and this is likely contributing to the small decrease in the N_2 formation rates (Fig. 8, S10-S11).

Based on the material balances given in Section 2.4 and the Supporting Information, the amounts of all N-containing species formed during TIH were estimated and results are provided in Table S1 (TIH without H_2O) and Table S2 (TIH with 5% H_2O). As the reaction temperature increases in the 200–400 °C range, the amount of NO(g) formed represents *inactive* NO_x-s, and this passes through a maximum at 300 °C (Fig. S15A). The amount of desirable N_2 gas product also passes through a maximum but at a higher temperature, ca. 350 °C (Fig. S15B). The amounts of N_2 and N_2O formed during TIH at 300 °C for the $Co_1Mg_2Al_1O_x$-LDO support alone (Fig. S12) were found to be very low (Table S1), and only a large amount of NO due to *NO_x-s decomposition* was formed. This result illustrates that Pt surface is necessary to offering active sites for di-hydrogen dissociation to form H-s. This species then diffuses towards the Pt-support interface (H-spillover process) responsible for NO_x-s reduction on the support.

The NO_x-s conversion (%) estimated via Eq. (S3) is referred to the NO_x-s adsorption step (0.1% NO/10% O_2/5% H_2O/1% Kr/He (T, 20 min)) followed by the H_2-reduction step (5% H_2/5% H_2O/He (T, t)), and results are presented in Fig. S16A. At the lowest temperature of 200 °C, the catalyst shows relatively low NO_x-s conversion ability (~ 10%), which increases significantly at 350 °C (~ 80%). A further increase of reaction T to 400 °C caused a drop of NO_x-s conversion to the value of ~ 60%. The presence of 5% H_2O in the H_2-containing reducing gas stream resulted in slightly lower NO_x-s conversion values (ca. < 7%). The effect of H_2O on the N_2-selectivity was also found to depend on reaction temperature (Fig. S16B). When T < 300 °C, water has a small negative effect on N_2-selectivity, while at T > 300 °C a small positive effect was observed.

Of interest was to compare the amount of NO_x-s formed after 20 min in 0.1% NO/10%O_2/5% H_2O/He (Fig. 6, 5% H_2O) with that corresponding to the N-containing species formed (NO, N_2 and N_2O) in the NO_x-reduction step (Table S1). It is seen that the former value is

significantly larger below 300 °C. This interesting result might be explained by considering the presence of some strongly bound nitrate/nitrite species which do not decompose to NO(g) at T < 300 °C. On the other hand, these species could be reached by spilt over H-s and get reduced. As shown in Table S1 for T = 200–250 °C, reduction of NO_x-s is not favored (very small amount of product). Thus, H diffusion on the present support seems not to be favorable at larger distances from the Pt-support interface at T < 300 °C. As reported by Savva and Efstathiou [24], surface diffusion of H-s species (formed on Pt) towards the MgO and CeO_2 support surfaces was limited within a region of ~ 4–5 Å around the Pt nanoparticles. This explained the fact that not all NO_x-s formed on the support surface could be activated in 5% H_2/He gas treatment. As shown in Table S3, the N_2-selectivity was found to be independent of GHSV, whereas the increase in NO_x-s conversion is due to the gradual decrease of GHSV.

3.3.2. *Effect of catalyst gas pretreatment (reduction vs calcination)*

The effect of gas pre-treatment (reduction vs calcination) of Pt/$Co_1Mg_2Al_1O_x$-LDO on the NO_x-s reduction step at 350 °C was evaluated under the same conditions as for the NO_x-s adsorption step (Fig. S8), and results are presented in Fig. S17 and Table S4. It is illustrated that the pre-reduced catalyst exhibits very similar rate profiles and NO_x-s conversion (ca. 74–77%) and N_2 selectivity values (ca. 83–84%). This very important result points out that *no catalyst pre-reduction step* by hydrogen is required before the next NO_x-s adsorption process step in the envisioned NO_x control for stationary applications (Scheme 1), thus contributing to the reduction of the operating cost with respect to hydrogen consumption. To provide some explanations on the above result (Fig. S17), the following are noted. The support used has a large NO_x-s storage capacity (Fig. S6, Table 1), and Pt surface sites are offered for NO oxidation to NO_2 (NO_x adsorption step). The latter is largely adsorbed on the support surface. During the reduction step, even in the presence of H_2O, there is enough fraction of Pt sites to form active H-s responsible for the reduction of NO_x-s (mainly on the support) via H-spillover. Therefore, even though Pt is largely oxidized under the NO_x storage step or after calcination, at the introduction of hydrogen over the catalyst there is a very quick reduction of sufficient PtO_x sites to Pt^0 to form H-s that spills over the support to actively participate in the reduction of adsorbed NO_x-s.

3.3.3. *Effect of hydrogen concentration on NO_x-s reduction*

Fig. 9A-D shows the effect of hydrogen concentration (0.5–5 vol%) on the evolution of the transient rates (μmol g^{-1} s^{-1}) of NO, N_2 and N_2O formation obtained during the reduction step of pre-adsorbed NO_x-s (20 min, 0.1 vol% NO/10 vol% O_2/5% H_2O/He gas treatment) at 350 °C over the Pt/$Co_1Mg_2Al_1O_x$-LDO catalyst. Since θ_H is expected to

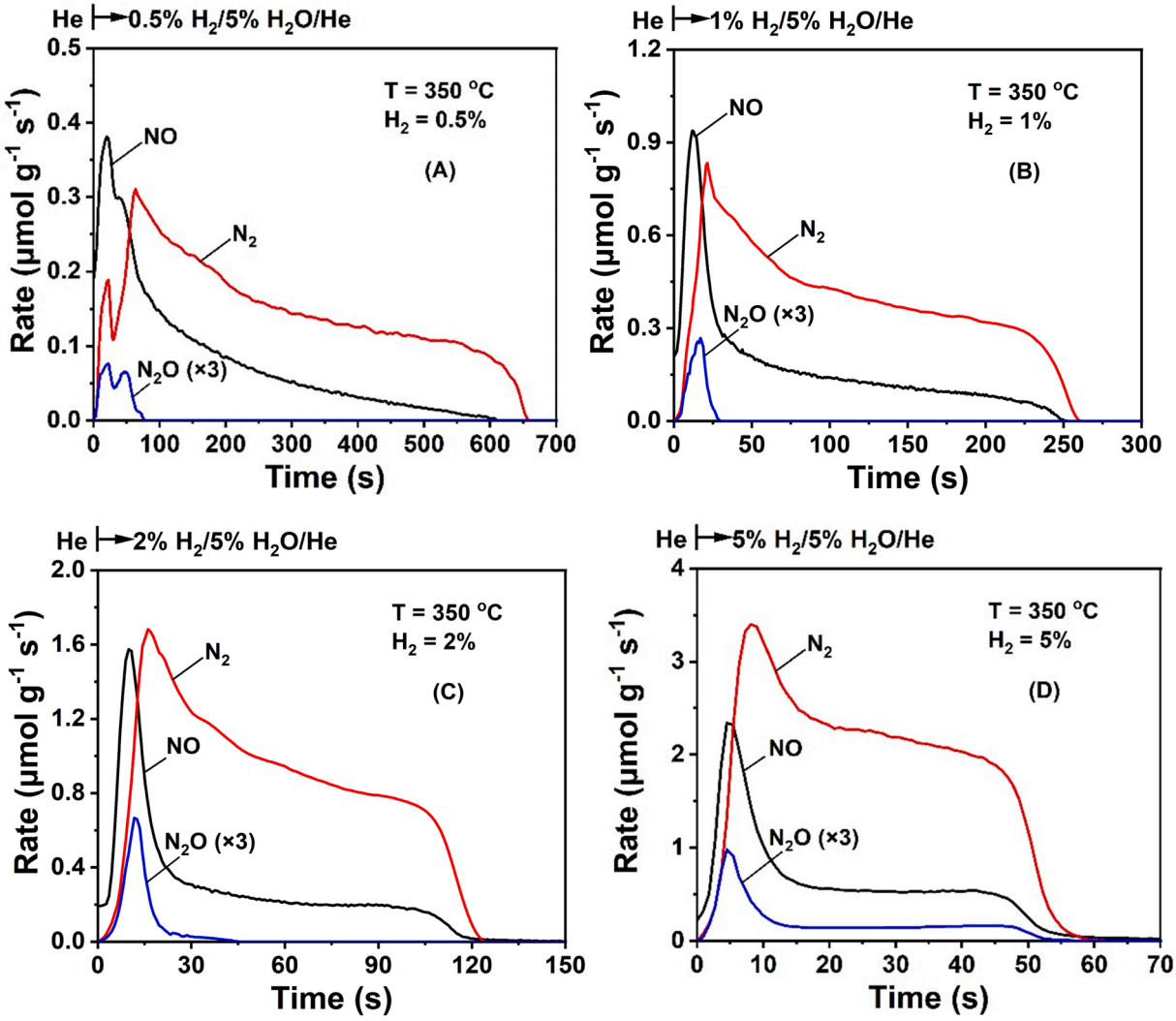

Fig. 9. Dynamic evolution of NO, N_2 and N_2O formation rates (μmol g^{-1} s^{-1}) obtained at 350 °C over the Pt/$Co_1Mg_2Al_1O_x$-LDO catalyst following the sequence of step-gas switches: 0.1% NO/10% O_2/5% H_2O/1% Kr/He (20 min) → He (3 min) → x vol% H_2/5% H_2O/He (t); x = 0.5, 1, 2 and 5. F_T = 50 NmL min^{-1}; W = 50 mg; GHSV = 60,000 h^{-1}.

be influenced by the hydrogen concentration in the gas phase, the latter is likely to affect the transient reduction kinetics of active NO_x-s and that of their decomposition to NO (inactive NO_x-s). As shown in Fig. 9A-D, the transient reduction and decomposition kinetics of NO_x-s strongly depend on the hydrogen gas concentration. When the latter is less or equal to 1 vol% (Fig. 9A, B), the time required to reach maximum NO_x-s reduction is significantly larger than that for H_2 concentrations higher than 1 vol% (Fig. 9C, D). The transient rates of N_2 and N_2O formation show the same trend as already discussed in Section 3.3.1. Broad shapes with low formation rates were obtained at lower hydrogen concentrations (ca. $\leq$ 1 vol%), while at higher concentrations, ca. 2–5 vol%, narrow profiles with increased reduction rates were obtained (note the change in the time scale in Fig. 9A-D). Table S5 provides the amounts (μmol g^{-1}) of NO, N_2 and N_2O formed during TIH at 350 °C for the different hydrogen concentrations used. When the hydrogen concentration is in the 0.5–5 vol% range, similar amounts of N_2 and N_2O are formed. These features suggest that the increase of hydrogen concentration enhanced the reduction rate of at least two different types of chemisorbed NO_x-s, and the hydrogen concentration only influenced the reduction rates for N_2 and N_2O formation but not the surface concentration of *active NO_x-s*. This led to similar N_2-selectivity (79–83%) and NO_x conversion (73–77%) values. It should be noted that at the switch to x vol%H_2/5%H_2O/He (t) at 350 °C (Fig. 9), the rate of NO formation is not zero since at the end of the 3-min He purge, some NO_x-s decomposition to NO(g) was still present.

3.3.4. *Effect of CO_2, H_2O and SO_2 on NO_x-s reduction*

Fig. 10 A shows the effect of 7% CO_2 and/or 5% H_2O on the estimated NO_x-s conversion and N_2-selectivity at 350 °C regarding the H_2 reduction step. It is seen that the NO_x-s conversion and N_2- selectivity are in the 76–85% and 81–85% range, respectively, showing that CO_2 and H_2O have a small only effect on the hydrogen reduction performance of the catalyst. Interestingly, even a small ~5% increase in NO_x-s conversion was observed when CO_2 was present in the H_2-containing reducing feed gas stream. Moreover, ~13% of CO_2 conversion to CO was measured due to the RWGS reaction, where CO might effectively reduce NO_x-s. The presence of both CO_2 and H_2O in the H_2-containing reducing feed gas stream resulted in the lowest NO_x-s conversion values, but this negative effect was small (~ 5%).

Fig. 10B shows the stability of NO_x-s conversion and N_2-selectivity following six consecutive SO_2-pretreatment cycles (see Section 3.2.4). It is seen that the hydrogen reduction performance of NO_x-s is quite stable after three cycles of SO_2 poisoning (50 ppm), and this is related to the good sulfur resistance of the catalyst. Finally, ~ 10% reduction in NO_x conversion and ~ 8% increase in N_2-selectivity were observed after six (Fig. 10B) and 12 (not shown) consecutive SO_2-poisoning cycles.

3.4. *Long-term NO_x storage/reduction cycling performance*

Fig. 11 shows a long-term (2 h) NSR performance test under periodic switching between NO_x storage (0.1% NO/10% O_2/5% H_2O/He, 3 min) and NO_x reduction by hydrogen (5% H_2/He, 1 min) reaction conditions at 350 °C (one NSR cycle takes 4 min). The duration of NO_x storage step was chosen based on the results presented in Fig. S8 (SI), where the NO slip was very small, while the duration of NO_x reduction in 5%H_2/He was based on the results presented in Fig. 8. It is seen that the NO (Fig. 11A), N_2 (Fig. 11B) and N_2O (Fig. 11C) transient responses remain practically constant throughout the cycling process (30 cycles). During the 1-min H_2 reduction step (H_2/He), sharp pulse-like responses of NO, N_2 and N_2O were formed immediately after the step-gas switch to 5% H_2/He (see also Fig. 8A-C). However, the magnitude of the NO and N_2O pulse-like responses (area under the pulse) were significantly smaller compared with that of N_2 gas formed (Fig. 11 C). The N_2 and N_2O formation is due to the reduction of NO_x (active species) formed during the 3-min chemisorption step, while the formation of NO under the 5%H_2/He gas treatment is related to the decomposition of inactive NO_x species (not leading to N_2/N_2O). The NO conversion and N_2 selectivity were estimated based on the following relationships:

$$\text{NO, conversion}(\%) = \frac{\int_{t_1}^{t_2} (NO_{in} - NO_{out})dt}{\int_{t_1}^{t_2} NO_{in}dt} \quad (16)$$

$$N_2\text{, selectivity}(\%) = \frac{\int_{t_1}^{t_2} N_2 dt}{\int_{t_1}^{t_2} (N_2 + N_2O)dt} \quad (17)$$

NO_{in} is the concentration of NO entering the reactor during the 3-min NO adsorption step, NO_{out} is the concentration of NO leaving the reactor during the whole 4-min cycling period, and t_1 and t_2 are the starting and ending times of each cycle (t_2-t_1 = 4 min). A NO_x conversion of ~ 92% and N_2-selectivity of ~ 97% were obtained for the applied NSR cycling performance test of 2 h.

3.5. *In-situ DRIFTS studies*

Fig. 12 presents IR bands in the 2450–2000 (Fig. 12A), 1750–1400 (Fig. 12B) and 1400–1100 cm^{-1} (Fig. 12C) ranges recorded after 20 min of reaction in 0.1% NO/10% O_2/He at 200 (curve a), 300 (curve b) and 400 °C (curve c) on the Pt/$Co_1Mg_2Al_1O_x$-LDO catalyst. The IR band at 2350 cm^{-1} (Fig. 12A) is assigned to nitrosyl species on Co^{2+} [61] (presence of Co_3O_4 phase in the support). The IR band at 2220 cm^{-1} is due to nitrosyl co-adsorbed with nitrate species on adjacent metal cation/oxygen anion site pairs of MgO support phase [22–24], and the IR bands at 2130 and 2075 cm^{-1} to adsorbed NO_2-s on metal cations present in the mixed metal oxide support, and of nitrosyls on the Pt surface, respectively [23,41,62]. The latter three IR bands largely decreased with increasing reaction temperature. In the IR region of 1700–1400 cm^{-1} (Fig. 12B), all the main IR bands (1633, 1558, 1547 and 1510 cm^{-1}) are associated with nitrite and/or nitrate species [22,23,41,62,63], while the main IR bands in the 1400–1100 cm^{-1} region (1285 and 1228 cm^{-1}, Fig. 12C) are due to bidentate and/or monodentate nitrate/nitrite and/or chelating nitrite species on support sites [22,62]. It is apparent (Fig. 12A-C) that the reaction temperature affects both the

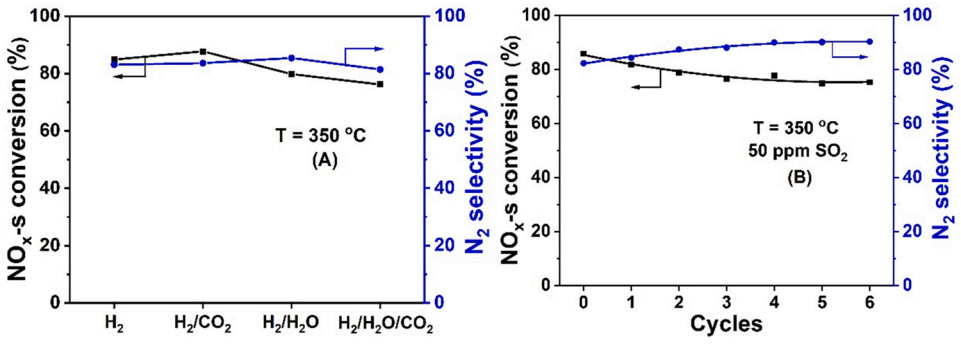

Fig. 10. NO_x-s conversion (left) and N_2-selectivity (right) at 350 °C under the H_2 reduction step according to the following sequence of step-gas switches: (A) 0.1% NO/10% O_2/5% H_2O/1% Kr/He (20 min) → He (3 min) → 5% H_2/CO_2 and/or H_2O/He (t) (7% CO_2 and 5% H_2O, when used) over the Pt/$Co_1Mg_2Al_1O_x$-LDO catalyst; (B) He → 50 ppm SO_2/1% Kr/He (20 min) → He (3 min) → 0.1% NO/10% O_2/1% Kr/He (20 min) → He (3 min) → 5% H_2/He (t) on the pre-sulfated catalyst. F_T = 50 N mL min^{-1}; W = 50 mg; GHSV = 60,000 h^{-1}.

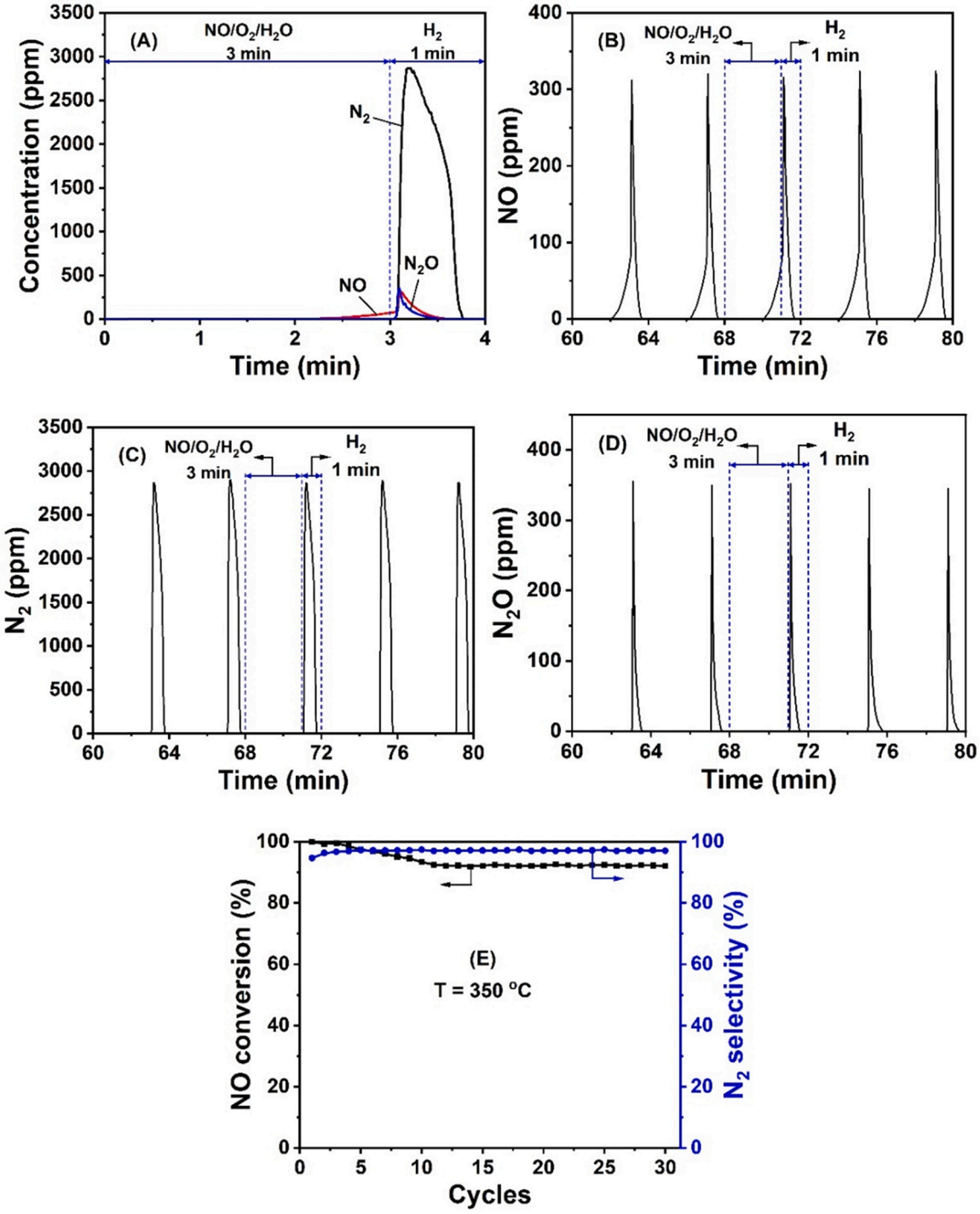

Fig. 11. (A) Dynamic evolution of NO, N_2 and N_2O concentration (ppm) obtained at 350 °C over the $Pt/Co_1Mg_2Al_1O_x$-LDO catalyst after the 1st NSR sequence of step-gas changes: 0.1% NO/10% O_2/5% H_2O/1% Kr/He (3 min) → 5% H_2/He (1 min) – 1st cycle. Dynamic evolution of NO (B), N_2 (C) and N_2O (D) concentration responses obtained during the 16th-20th NSR cycles, and (E) NO-conversion (%) and N_2-selectivity (%) of the NSR process for 30 continuous cycles (2 h total duration). F_T = 50 N mL min^{-1}; W = 50 mg; GHSV = 60,000 h^{-1}.

concentration (integral infrared area) and the structure of adsorbed NO_x formed on the support and Pt surfaces.

Fig. S18 shows IR bands in the 2450–2000 (Fig. S18A), 1750–1400 (Fig. S18B), and 1400–1100 cm^{-1} (Fig. S18C) ranges recorded after 20 min in 0.1 vol% NO/10 vol% O_2/He gas mixture at 200 °C, and during transient isothermal hydrogenation with 5% H_2/He (t) (TIH, NO_x-s reduction step), following NO/O_2/He gas treatment. Similar DRIFTS spectra were recorded at 300 °C (Fig. S19). The spectra marked "0 s" are referred to the 20-min NO/O_2/He gas treatment just before the 5%H_2/He gas switch. All adsorbed NO_x identified under the NO/O_2/He gas treatment appear *active* intermediates at 200 °C and were fully reduced in ~ 1 min in the 5%H_2/He gas stream, except the nitrosyl species co-adsorbed with nitrate on the MgO support and those of adsorbed $NO_2^{\delta+}$ associated with metal cations of the support (Fig. S18A). By increasing the reduction temperature to 300 °C in 5%H_2/He, the intensity of all IR bands dropped significantly for the same time on hydrogen stream (Fig. S19). This result is in harmony with the corresponding TIH-Mass spectrometry transient evolution responses of the

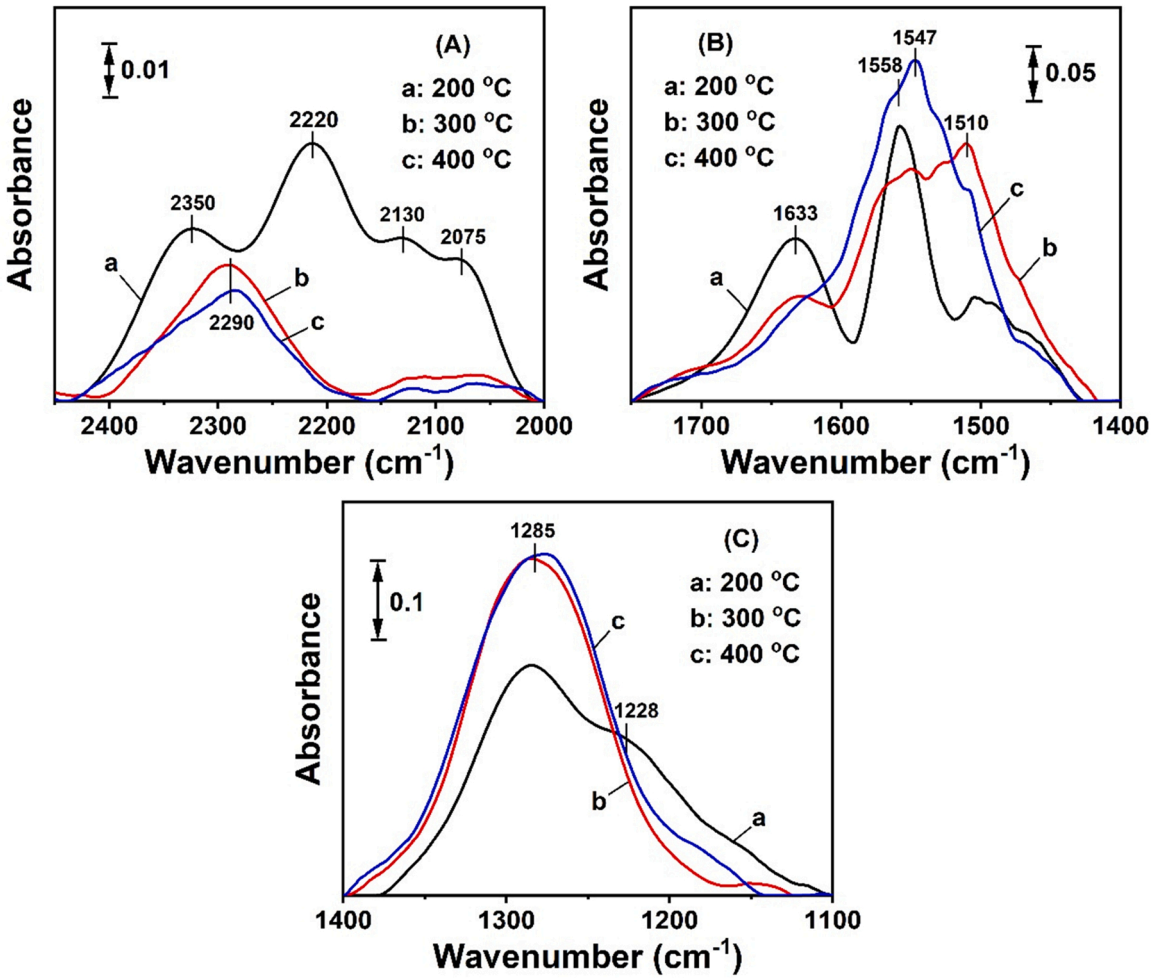

Fig. 12. *In-situ* NO-DRIFTS spectra recorded in the (A) 2450 – 2000, (B) 1750 – 1400, and (C) 1400 – 1100 cm^{-1} ranges after 20 min in 0.1% NO/10% O_2/He gas flow at 200, 300 and 400 °C over the $Pt/Co_1Mg_2Al_1O_x$-LDO catalyst.

gas-phase species formed after hydrogenation of NO_x-s (Fig. 8A, C). The results shown in Fig. S18A confirm the quantitative results of TIH-Mass spectrometry reported in Tables S1 and S2, where at 200 °C, a large part of the formed NO_x-s cannot react with hydrogen. The chemical composition of these *inactive NO_x-s* species was mentioned above.

4. Conclusions

The 0.59 wt% $Pt/Co_1Mg_2Al_1O_x$-LDO catalytic system presented in this work showed a potential for the control of NO_x emissions from stationary sources using a "swing-reactor" system of two catalytic fixed bed reactors after implementation of the NO_x adsorption / NO_x reduction by hydrogen design concept. Through a series of step-gas concentration switches under practical feed gas compositions (presence of CO_2 and H_2O and 20 or 50 ppm SO_2) for the NO_x adsorption and reduction process steps, the transient kinetics of NO_x-s storage and reduction by hydrogen were evaluated, aiming to reveal its potential application as a NSR catalytic system consisting of low precious metal loading (ca. less than 0.6 wt%) and a passive NO_x adsorbent. The following conclusions can be derived from the results of this work:

(a) The transient kinetics of NO_x-s storage in the presence of O_2 (NO/O_2/He feed gas stream) was found to be largely different than that obtained in the NO/He feed gas stream. NO decomposition was completely inhibited by the presence of oxygen, and NO oxidation plays a key role in the significant improvement of NO_x storage capacity. Pt surface is responsible for the formation of an appropriate coverage of atomic oxygen, able to promote NO oxidation to NO_2. This is then transferred to appropriate adsorption sites on the $Co_1Mg_2Al_1O_x$-LDO support, thus enhancing the NO_x storage capacity (NSC) of the solid. At 300 °C, NSC was increased by a factor of ~ 3.7 under the 0.1%NO/10% O_2/He gas mixture compared with the 0.1%NO/He one. The NSC vs temperature relationship passed through a maximum at 300 °C in the 200–400 °C range.

(b) Both H_2O and CO_2 showed a negative effect on the NO_x-s storage performance at a low temperature (ca. 200 °C). On the other hand, at higher temperatures (ca. 350–400 °C), the negative influence of water is weakened and becomes slightly positive. When H_2O and CO_2 were co-fed in the NO_x feed gas stream, the NO_x-s storage performance remained practically the same as that obtained in the absence of CO_2 or H_2O in the feed.

(c) The transient isothermal hydrogenation (TIH, NO_x-s reduction step) of adsorbed NO_x-s (formed via $NO/O_2/H_2O$/He gas treatment), most of which reside on the LDO support, involves NO_x-s reduction to N_2 and to a small only extent reduction to N_2O. This reduction step proceeds mainly via H-spillover from Pt to the NO_x-s adsorption sites of the support. TIH and in-situ DRIFTS experiments illustrated that a small part of adsorbed NO_x on the catalyst surface cannot be fast reacted by hydrogen at temperatures lower than 250 °C. At higher temperatures, practically all NSC can be regenerated by hydrogen with N_2-selectivities larger than 80%. Hydrogen concentration in the 0.5–5 vol% range does not influence the amount of reduced NO_x-s but only the rate of

their reduction, thus the regeneration time. The latter was found to decrease with increasing H_2 concentration in the feed.

(d) Small negative effects when 5 vol% H_2O or 5 vol% H_2O/7 vol% CO_2 were present in the H_2-containing feed gas stream on the NO_x-s reduction by H_2 performance at 350 ^oC were found.

(e) Pretreatment of catalyst with 50 ppm SO_2/He gas mixture for 20 min, followed by NO/O_2/He (20 min) and H_2/He (10 min) – one cycle, showed a decrease by 16.3% of NO_x-s adsorption capacity and by 4.7% of NO_x-s reacted by H_2 compared with the case of no SO_2/He gas pretreatment. Twelve consecutive cycles of SO_2 gas pretreatment – NO_x adsorption/NO_x-s reduction by H_2, revealed an excellent stability of catalyst's performance in terms of NO_x-s conversion (~80%) and N_2-selectivity (~90%).

(f) A catalyst reduction or calcination step applied between consecutive swing cycles (NO_x-reduction followed by NO_x-s adsorption) showed very similar NSR performances for the present catalytic system. This important result is expected to reduce the operating cost of the NSR technology (Scheme 1) via the significantly lower amounts of hydrogen required.

(g) The excellent long-term cycling stability (2 h) between NO_x-storage (3 min) followed by NO_x-reduction in hydrogen (1 min) demonstrated the practical potential of the NSR process for stationary NO_x control applications.

CRediT authorship contribution statement

Cheng Zhang: Validation, Investigation, Writing – original draft and Revisions; **Constantinos M. Damaskinos**: Validation; **Michalis A. Vasiliades:** Validation; **Yuefeng Liu**: Validation; **Qian Jiang**: Validation; **Qiang Wang**: Investigation, Supervision; **Angelos M. Efstathiou:** Methodology, Supervision, Writing – original, Final Draft and Revisions.

Declaration of Competing Interest

The authors declare that they have no known competing financial interests or personal relationships that could have appeared to influence the work reported in this paper.

Data Availability

Data will be made available on request.

Acknowledgements

We acknowledge the Fundamental Research Funds for the National Natural Science Foundation of China (U1810209 and 52225003), the Beijing Municipal Education Commission via the Innovative Transdisciplinary Program "Ecological Restoration Engineering", the LiaoNing Revitalization Talents Program (XLYC1907053), and the CAS Youth Innovation Promotion Association (2018220) for their financial support. The authors also acknowledge Hiroaki Matsumoto for the STEM analysis. The China Scholarship Council (202006510039), and the Research Committee of the University of Cyprus are also acknowledged for their financial support.

Appendix A. Supporting information

Supplementary data associated with this article can be found in the online version at doi:10.1016/j.apcatb.2023.122455.

References

[1] R. Villamaina, U. Iacobone, I. Nova, E. Tronconi, M.P. Ruggeri, L. Mantarosie, J. Collier, D. Thompsett, Mechanistic insight in NO trapping on Pd/Chabazite systems for the low-temperature NO_x removal from Diesel exhausts, Appl. Catal. B Environ. 284 (2021), 119724.

[2] S. Roy, A. Baiker, NO_x storage-reduction catalysis: from mechanism and materials properties to storage-reduction performance, Chem. Rev. 109 (2009) 4054–4091.

[3] J.R. González-Velasco, R. López-Fonseca, B. Pereda-Ayo, N.S.R. Technology, in NOx Trap Catalysts and Technologies, Fundamentals and Industrial Applications (L. Lietti, L. Castodi, Eds), Catalysis 33 (2018) 36–66.

[4] B. Choi, K. Lee, G. Son, Review of recent after-treatment technologies for de-NO_x process in diesel engines, Int. J. Automot. Technol. 21 (6) (2020) 1597–1618.

[5] Y. Cui, Q. Yan, C. Zhang, L. Qiu, Q. Wang, Pt/Ba/$Co_1Mg_2Al_1O_x$ with dual adsorption sites: a novel NO_x storage and reduction catalyst, Catal. Commun. 101 (2017) 125–128.

[6] R. Yang, Y. Cui, Q. Yan, C. Zhang, L. Qiu, D. O'Hare, Q. Wang, Design of highly efficient NO_x storage-reduction catalysts from layered double hydroxides for NO_x emission control from naphtha cracker flue gases, Chem. Eng. J. 326 (2017) 656–666.

[7] C.N. Costa, P.G. Savva, J.L.G. Fierro, A.M. Efstathiou, Industrial H_2-SCR of NO on a novel Pt/MgO-CeO_2 catalyst, Appl. Catal. B: Environ. 75 (2007) 147–156.

[8] K. Polychronopoulou, A.M. Efstathiou, NO_x control via H_2-selective catalytic reduction (H_2-SCR) technology for stationary and mobile applications, Recent Pat. Mater. Sci. 5 (2012) 87–104.

[9] A.N. Zagoruiko, L.N. Bobrova, N. Vernikovskaya, S. Zazhigalov, Unsteady-state operation of reactors with fixed catalyst beds, Rev. Chem. Eng. 37 (1) (2021) 193–225.

[10] A.S. Noskov, L.N. Bobrova, G.A. Bunimovich, O.V. Goldman, A.N. Zagoruiko, Y. S. Matros, Application of the nonstationary state of a catalyst surface for gas purification from toxic impurities, Catal. Today 27 (1996) 315–319.

[11] A.W.-L. Ting, M.P. Harold, V. Balakotaiah, Elucidating the mechanism of fast cycling NO_x storage and reduction using C_3H_6 and H_2 as reductants, Chem. Eng. Sci. 189 (2018) 413–421.

[12] A.M. Efstathiou, V.N. Stathopoulos, Lean Burn DeNO_x applications: Stationary and Mobile Sources, Wiley-VCH Verlag GmbH & Co. KGaA,, 2015.

[13] A. Bueno-López, D. Lozano-Castelló, J.A. Anderson, NO_x storage and reduction over copper-based catalysts. Part 1: BaO+CeO_2 supports, Appl. Catal. B: Environ. 198 (2016) 189–199.

[14] X. Wang, Y. Yu, H. He, Effect of Co addition to Pt/Ba/Al_2O_3 system for NO_x storage and reduction, Appl. Catal. B Environ. 100 (2010) 19–30.

[15] Y. Zhang, R. You, D. Liu, C. Liu, X. Li, Y. Tian, Z. Jiang, S. Zhang, Y. Huang, Y. Zha, M. Meng, Carbonates-based noble metal-free lean NO trap catalysts MO-K_2CO_3/$K_2Ti_8O_{17}$ (M = Ce, Fe, Cu, Co) with superior catalytic performance, Appl. Surf. Sci. 357 (2015) 2260–2276.

[16] J.A. Onrubia-Calvo, B. Pereda-Ayo, U. De-La-Torre, J.R. González-Velasco, Strontium doping and impregnation onto alumina improve the NO_x storage and reduction capacity of $LaCoO_3$ perovskites, Catal. Today 333 (2019) 208–218.

[17] C.N. Costa, A.M. Efstathiou, Low-temperature H_2-SCR of NO on a novel Pt/MgO-CeO_2 catalyst, Appl. Catal. B Environ. 72 (2007) 240–252.

[18] A. Wang, L. Ma, Y. Cong, T. Zhang, D. Liang, Unique properties of Ir/ZSM-5 catalyst for NO reduction with CO in the presence of excess oxygen, Appl. Catal. B Environ. 40 (2003) 319–329.

[19] J. Lin, B. Qiao, N. Li, L. Li, X. Sun, J. Liu, X. Wang, T. Zhang, Little do more: a highly effective Pt_1/FeO_x single-atom catalyst for the reduction of NO by H_2, Chem. Commun. 51 (2015) 7911–7914.

[20] C.O. Bennett, Experiments and processes in the transient regime for heterogeneous catalysis, Adv. Catal. 44 (1999) 329–416 (and references therein).

[21] A.M. Efstathiou, Elucidation of mechanistic and kinetic aspects of water-gas shift reaction on supported Pt and Au catalysts via transient isotopic techniques, Catalysis 28 (2016) 175–236 (and references therein).

[22] C.N. Costa, A.M. Efstathiou, Mechanistic aspects of the H_2-SCR of NO on a novel Pt/MgO-CeO_2 catalyst, J. Phys. Chem. C 111 (2007) 3010–3020.

[23] C.N. Costa, A.M. Efstathiou, Transient isotopic kinetic study of the NO/H_2/O_2 (Lean de-NO_x) reaction on Pt/SiO_2 and Pt/La-Ce-Mn-O catalysts, J. Phys. Chem. B 108 (2004) 2620–2630.

[24] P.G. Savva, A.M. Efstathiou, The influence of reaction temperature on the chemical structure and surface concentration of active NO_x in H_2-SCR over Pt/MgO-CeO_2: SSITKA-DRIFTS and transient mass spectrometry studies, J. Catal. 257 (2008) 324–333.

[25] W. Hua, R. Zou, Y. Dong, S. Zhang, H. Song, S. Liu, C. Zheng, I. Nova, E. Tronconi, X. Gao, Synergy of vanadia and ceria in the reaction mechanism of low-temperature selective catalytic reduction of NO_x by NH_3, J. Catal. 391 (2020) 145–154.

[26] F. Gramigni, N.D. Nasello, N. Usberti, U. Iacobone, T. Selleri, W. Hu, S. Liu, X. Gao, I. Nova, E. Tronconi, Transient kinetic analysis of low-temperature NH_3-SCR over Cu-CHA catalysts reveals a quadratic dependence of Cu reduction rates on Cu^{II}, ACS Catal. 11 (2021) 4821–4831.

[27] I. Nova, L. Lietti, L. Castoldi, E. Tronconi, P. Forzatti, New insights in the NO_x reduction mechanism with H_2 over Pt-Ba/γ-Al_2O_3 lean NO_x trap catalysts under near-isothermal conditions, J. Catal. 239 (2006) 244–254.

[28] D. Mráček, P. Kočí, M. Marek, J.-S. Choi, J.A. Pihl, W.P. Partridge, Dynamics of N_2 and N_2O peaks during and after the regeneration of lean NO trap, Appl. Catal. B Environ. 166–167 (2015) 509–517.

[29] L. Castoldi, R. Matarrese, L. Lietti, S. Morandi, M. Daturi, Mechanistic Aspects of the Reduction of the Stored NO_x by H_2 Investigated by Isotopic Labelling Experiments and FTIR Spectroscopy, in NO_x Trap Catalysis and Technologies, Fundamentals and Industrial Applications (L. Lietti, L. Castoldi, Eds), Catalysis Series No. 33, RSC, 2018, pp 187–212.

[30] R.S. Larsona, V.K. Chakravarthy, J.A. Pihl, C.S. Daw, Microkinetic modeling of lean NO_x trap chemistry, Chem. Eng. J. 189–190 (2012) 134–147.

[31] T. Lesage, C. Verrier, P. Bazin, J. Saussey, M. Daturi, Studying the NO_x-trap mechanism over a Pt-Rh/Ba/Al_2O_3 catalyst by operando FT-IR spectroscopy, Phys. Chem. Chem. Phys. 5 (2003) 4435–4440.
[32] Q. Yan, Y. Gao, Y. Li, M.A. Vasiliades, S. Chen, C. Zhang, R. Gui, Q. Wang, T. Zhu, A.M. Efstathiou, Promotional effect of Ce doping in Cu_4Al_1Ox-LDO catalyst for low-T practical NH_3-SCR: Steady-state and transient kinetics studies, Appl. Catal. B Environ. 255 (2019), 117749.
[33] C.M. Kalamaras, K.C. Petallidou, A.M. Efstathiou, The effect of La^{3+}-doping of CeO_2 support on the water-gas shift reaction mechanism and kinetics over Pt/$Ce_{1-x}La_xO_{2-\delta}$, Appl. Catal. B Environ. 136–137 (2013) 225–238.
[34] C.N. Costa, S.Y. Christou, G. Georgiou, A.M. Efstathiou, Mathematical modeling of the oxygen storage capacity phenomenon studied by CO pulse transient experiments over Pd/CeO_2 catalyst, J. Catal. 219 (2003) 259–272.
[35] B.J. Kip, F.B.M. Duivenvoorden, D.C. Koningsberger, R. Prins, Determination of metal particle size of highly dispersed Rh, Ir, and Pt catalysts by hydrogen chemisorption and EXAFS, J. Catal. 105 (1987) 26–38.
[36] P. Trens, R. Durand, B. Coq, C. Coutanceau, S. Rousseau, C. Lamy, Poisoning of Pt/C catalysts by CO and its consequences over the kinetics of hydrogen chemisorption, Appl. Catal. B Environ. 92 (2009) 280–284.
[37] C. Prado-Burguete, A. Linares-Solano, F. Rodriguez-Reinoso, C. Salinas-Martinez De Lecea, Effect of carbon support and mean Pt particle size on hydrogen chemisorption by carbon-supported Pt catalysts, J. Catal. 128 (1991) 397–404.
[38] S. Bernal, M.A. Cauqui, G.A. Cifredo, J.M. Gatica, C. Larese, J.A.P. Omil, Chemical and microstructural investigation of Pt/CeO_2 catalysts reduced at temperatures ranging from 473 to 973 K, Catal. Today 29 (1996) 77–81.
[39] J.T. Miller, B.L. Meyers, F.S. Modica, G.S. Lane, M. Vaarkamp, D.C. Koningsberger, Hydrogen temperature-programmed desorption (H_2 TPD) of supported platinum catalysts, J. Catal. 143 (1993) 395–408.
[40] J. Raskó, CO-induced surface structural changes of Pt on oxide-supported Pt catalysts studied by DRIFTS, J. Catal. 217 (2003) 478–486 (and references therein).
[41] E. Ivanova, M. Mihaylov, F. Thibault-Starzyk, M. Daturi, K. Hadjiivanov, FTIR spectroscopy study of CO and NO adsorption and co-adsorption on Pt/TiO_2, J. Mol. Catal. A: Chem. 274 (2007) 179–184.
[42] J. Luo, M. Meng, Y. Zha, Y. Xie, T. Hu, J. Zhang, T. Liu, A comparative study of Pt/Ba/Al_2O_3 and Pt/Fe-Ba/Al_2O_3 NSR catalysts: New insights into the interaction of Pt-Ba and the function of Fe, Appl. Catal. B Environ. 78 (2008) 38–52.
[43] Z. Zhang, M. Crocker, B. Chen, Z. Bai, X. Wang, C. Shi, Pt-free, non-thermal plasma-assisted NO storage and reduction over M/Ba/Al_2O_3 (M = Mn, Fe, Co, Ni, Cu) catalysts, Catal. Today 256 (2015) 115–123.
[44] L. Righini, L. Kubiak, S. Morandi, L. Castoldi, P. Forzatti, n-Heptane as a reducing agent in the NO_x removal over a Pt-Ba/Al_2O_3 NSR catalyst, ACS Catal. 4 (2014) 3261–3272.
[45] S. Andonova, V. Marchionni, L. Lietti, L. Olsson, Micro-calorimetric studies of NO_2 adsorption on Pt/BaO-supported on γ-Al_2O_3 NO_x storage and reduction (NSR) catalysts-Impact of CO_2, J. Mol. Catal. 436 (2017) 43–52.
[46] L. Lietti, P. Forzatti, I. Nova, E. Tronconi, NO_x storage reduction over Pt-Ba/γ-Al_2O_3 catalyst, J. Catal. 204 (2001) 175–191.
[47] W. Li, K. Sun, Z. Hu, B. Xu, Characteristics of low platinum Pt-BaO catalysts for NO_x storage and reduction, Catal. Today 153 (2010) 103–110.
[48] C.M.L. Scholz, V.R. Gangwal, M.H.J.M. de Croon, J.C. Schouten, Influence of CO_2 and H_2O on NO_x storage and reduction on a Pt-Ba/γ-Al_2O_3 catalyst, Appl. Catal. B Environ. 71 (2007) 143–150.
[49] J. Wang, X. Mei, L. Huang, Q. Zheng, Y. Qiao, K. Zang, S. Mao, R. Yang, Z. Zhang, Y. Gao, Z. Guo, Z. Huang, Q. Wang, Synthesis of layered double hydroxides/graphene oxide nanocomposite as a novel high-temperature CO_2 adsorbent, J. Energy Chem. 24 (2015) 127–137.
[50] V. Alcalde-Santiago, A. Davó-Quiñonero, I. Such-Basáñez, D. Lozano-Castelló, A. Bueno-López, Macroporous carrier-free Sr-Ti catalyst for NO_x storage and reduction, Appl. Catal. B Environ. 220 (2018) 524–532.
[51] T. Yu, J. Wang, M. Shen, J. Wang, W. Li, The influence of CO_2 and H_2O on selective catalytic reduction of NO by NH_3 over Cu/SAPO-34 catalyst, Chem. Eng. J. 264 (2015) 845–855.
[52] T.T. Yang, H.T. Bi, X. Cheng, Effects of O_2, CO_2 and H_2O on NO_x adsorption and selective catalytic reduction over Fe/ZSM-5, Appl. Catal. B Environ. 102 (2011) 163–171.
[53] S. Hodjati, P. Bernhardt, C. Petit, V. Pitchon, A. Kiennemann, Removal of NO_x: Part II. Species formed during the sorption/desorption processes on barium aluminates, Appl. Catal. B Environ. 19 (1998) 221–232.
[54] A. Kumar, V. Medhekar, M.P. Harold, V. Balakotaiah, NO decomposition and reduction on Pt/Al_2O_3 powder and monolith catalysts using the TAP reactor, Appl. Catal. B Environ. 90 (2009) 642–651.
[55] R. Burch, P.J. Millington, A.P. Walker, Mechanism of the selective reduction of nitrogen monoxide on platinum-based catalysts in the presence of excess oxygen, Appl. Catal. B Environ. 4 (1994) 65–94.
[56] D. Mei, Q. Ge, M. Neurock, L. Kieken, J. Lerou, First-principles-based kinetic Monte Carlo simulation of nitric oxide decomposition over Pt and Rh surfaces under lean-burn conditions, Mol. Phys. 102 (2004) 361–369.
[57] C.K. Narula, L.F. Allard, G.M. Stocks, M. Moses-DeBusk, Remarkable NO oxidation on single supported platinum atoms, Sci. Rep. 4 (2014) 7238.
[58] Z. Savva, K.C. Petallidou, C.M. Damaskinos, G.G. Olympiou, V.N. Stathopoulos, A. M. Efstathiou, H_2-SCR of NO_x on low-SSA CeO_2-supported Pd: The effect of Pd particle size, Appl. Catal. A: Gen. 615 (2021), 118062.
[59] P. Forzatti, L. Lietti, L. Castoldi, Storage and reduction of NO_x over LNT catalysts, Catal. Lett. 145 (2015) 483–504.
[60] D.D. Hibbitts, R. Jiménez, M. Yoshimura, B. Weiss, E. Iglesia, Catalytic NO activation and NO-H_2 reaction pathways, J. Catal. 319 (2014) 95–109.
[61] M.-J. Kim, S.-J. Lee, In-Soo Ryu, S.-H. Moon, M.-W. Jeon, C.H. Ko, S.G. Jeon, Understanding the effect of NO adsorption on potassium-promoted Co_3O_4 for N_2O decomposition, Catal. Lett. 147 (2017) 2886–2892.
[62] K.I. Hadjiivanov, Identification of neutral and charged N_xO_y surface species by IR spectroscopy, Catal. Rev. 42 (2000) 71–144.
[63] A. Bourane, O. Dulaurent, S. Salasc, C. Sarda, C. Bouly, D. Bianchi, Heats of adsorption of linear NO species on a Pt/Al_2O_3 catalyst using in situ infrared spectroscopy under adsorption equilibrium, J. Catal. 204 (2001) 77–88.